Oceanography and Acoustics
Editors: Allan R. Robinson and Ding Lee
AIP Press (1994)

3. Surface-Duct Propagation and the Ocean Mixed Layer

M. Porter, S. Piacsek, L. Henderson and F. Jensen†

3.1. Introductory Remarks

The surface layers of the ocean form a part of the ocean-atmosphere boundary layer system, and as such are dominated by turbulent mixing processes and the air-sea heat and momentum fluxes. These layers are referred to collectively as the "mixed layer" because there is almost always present at least one homogeneous layer near the surface in which the temperature and salinity profiles are constant with depth (the result of mixing), and the sound velocity increases with depth due to pressure effects. The bottom of the mixed layer then most often represents the surface maximum of the sound velocity profile.

From the point of view of acoustic modeling, the mixed layer leads to a surface duct which can drastically alter the propagation of sound in the ocean. Mixed-layer models provide the details of the sound speed profile which are required for acoustic modeling. In a sense, they may be considered as sophisticated interpolators which provide the sound speed between times of, for example, two weeks, when it might be practical to measure directly the mixed-layer structure. Between measurements, the mixed-layer structure is tracked by taking account of the surface wind and heat flux at the ocean-air interface.

Normally, mixed layers are of interest only for the propagation of high-frequency sound, since there is a low-frequency cut-off below which the surface duct has negligible effect. However, at higher latitudes, for example at the locations of the weather ships Lima (57N,20W) and Charlie (53N,36W) in the Northeast Atlantic, mixed-layer depths of 300–400 m have been observed consistently in the December to April period [Warn-Varnas *et al.*, 1986]. Mixed layers of such depth influence even sound waves of lower frequencies, for example 200 Hz or so.

While a great deal of work has been spent on mixed-layer models and acoustic models, a fundamental issue remains: mixed-layer models are principally validated on the basis of how well they match a measured temperature profile; however, a measure of "goodness of fit" is difficult to motivate. For instance, if one

† An abbreviated version of this paper appeared in the Proceedings of the Second IMACS Symposium on Computational Acoustics [Porter *et al.*, 1990].

model provides a more accurate prediction of mixed-layer depth and another provides a more accurate prediction of mixed-layer temperature, then which should be preferred?

Many times, however, the situation is more complicated, in that the "mixed layer" is actually composed of a sandwich of several homogeneous layers, each the result of different mixing, cooling and heating epochs on the diurnal, synoptic (i.e., weather) and seasonal time-scales, or any combination of these. (Throughout this paper we shall use the term "mixed layer" in this broader sense.) Since the ultimate objective is to provide an accurate transmission loss calculation, it is natural to make a judgment based on this same consideration.

The outline of this paper is as follows. In sections 3.2 and 3.3, we provide a brief overview of mixed-layer models and acoustic models, respectively. In section 3.4, we compare the performance of the various acoustic models in a particular mixed-layer environment. In section 3.5, we consider which parameters of the mixed layer are most important to provide an accurate prediction of transmission loss. In particular, we address the sensitivity of transmission loss to offsets in the mixed-layer temperature, to errors in the gradient of temperature, and errors in mixed-layer depth. (For a good summary of errors which affect mixed-layer modeling, we refer the reader to Heathershaw and Codd [1986].) Next, in section 3.6, we examine the implications using a particular mixed-layer model compared to climatology and to direct XBT measurements which provide "ground truth." In section 3.7, we examine differences in particular mixed-layer models and finally, we end with a summary and conclusions in section 3.8.

3.2. The Mixed-Layer Models

The nature of the boundary layer of the near-surface layers has strong implications for the models designed to simulate them. The principal requirement for these models is the correct specification of the fluxes of momentum and heat across the air-sea interface, and the correct simulation of the turbulent mixing due to surface wave breaking and shear of the wind-driven currents. The latter is particularly important near the bottom of the mixed layer, and is usually referred to as the entrainment zone.

Due to the very large discrepancy in spatial scales between the horizontal extent of atmospheric cyclones and the depth of the mixed layer, mixed-layer models have been generally constructed as 1-D models, with pressure gradients and all horizontal gradients neglected. These assumptions are very similar to the usual boundary layer approximations in hydrodynamics.

The scenario is illustrated in Fig. 3.1. The ocean surface is irradiated by the sun, taking into account blockage by cloud cover. The winds provide a surface stress which drives the mean flow in the mixed layer. The dependent variables are then the temperature (T) and salinity (S), and the two components of horizontal velocity (U, V) as a function of depth (z).

The evolution of these quantities is predicted by solving a set of coupled nonlinear partial differential equations. In particular, the principal balance in the equations of motion comes from a balance of acceleration, vertical diffusion

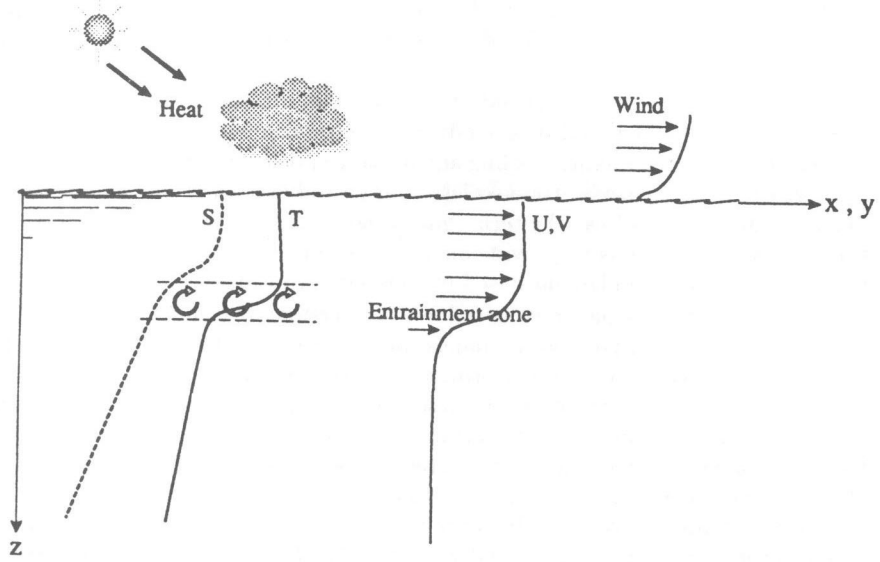

FIG. 3.1. Scenario for the mixed-layer models.

and the Coriolis force due to the earth's rotation:

$$\frac{\partial U}{\partial t} = \frac{\partial}{\partial z}\left(K_m \frac{\partial U}{\partial z}\right) + 2\Omega V, \tag{3.1}$$

$$\frac{\partial V}{\partial t} = \frac{\partial}{\partial z}\left(K_m \frac{\partial V}{\partial z}\right) - 2\Omega U, \tag{3.2}$$

where U and V are the E-W and N-S components of the velocity, Ω is the rotation rate of the earth (7×10^{-5} sec^{-1}) and K_m is the coefficient of turbulent momentum diffusion. The transport equation for heat balances vertical diffusion of heat and incident solar radiation q_s in 1-D models, and also advection of heat in 3-D models. Thus,

$$\frac{\partial T}{\partial t} = \frac{\partial}{\partial z}\left(K_h \frac{\partial T}{\partial z}\right) + (\mathbf{U} \cdot \nabla)T + q_s, \tag{3.3}$$

where T is the temperature. There is similarly a transport equation for salt,

$$\frac{\partial S}{\partial t} = \frac{\partial}{\partial z}\left(K_s \frac{\partial S}{\partial z}\right) + (\mathbf{U} \cdot \nabla)S, \tag{3.4}$$

where K_h and K_s are turbulent diffusion coefficients for heat and salt, respectively, and S is salinity.

The derivation of the transport equations above involves generalized closure methods commonly used in the simulation of turbulent flows to relate the small-scale motions to the mean flow. An excellent review of these methods for geophysical flows is given by Mellor and Yamada [1982]. Applying different order

turbulence closures one obtains formulas for the diffusion coefficients which can be simple functional forms involving U, V, T, and S or can involve the solution of additional evolution equations. A fuller discussion of higher-order closures applied to mixed-layer modeling may be found in Warn-Varnas and Piacsek [1979] and Klein and Coantic [1981].

At this point we must introduce the concept of "profile" models (also called "diffusive" or "differential") and "bulk" (or "integrated") models. The profile models solve the differential equations (3.1)–(3.4) directly on a finite difference grid yielding predictions of the evolution of the mixed layer in detail as a function of time and depth. The Mellor-Yamada model (see Mellor and Yamada [1974] and Martin [1985]) considered in this chapter is a profile-type model, estimating the turbulent diffusion coefficients K_m, K_h and K_s with various degrees of turbulence closure, known as the "Level 2, 2.5, etc." model.

In contrast, bulk models make the additional assumption that the mixed layer is uniform and predict its evolution in a depth-integrated sense, using the depth-integrated versions of Eqs. (3.1)–(3.4). Momentum and heat added via entrainment at the surface and bottom are assumed to be distributed uniformly throughout the mixed layer. The turbulence closure approximations are invoked to arrive at the proper formulas for the respective entrainment rates. For a concise summary of these approximations the reader is referred to Martin [1985].

The bulk models considered in this paper will be the Niiler model [Niiler, 1975, Davis *et al.*, 1981], and the Garwood model [Garwood, 1977]. The bulk and profile models provide somewhat different predictions of the mixed-layer development over time. An intermodel comparison was performed by Martin [1985], where observed fluxes and hydrography were used for the evaluation at the two weather ship sites Papa and November in the North Pacific. In general, it was found that bulk-type mixed-layer models mix much deeper than "differential" models.

Recently, advances have been made in two directions in turbulent mixed-layer modeling in the ocean. In one attempt, the effects of rotation on stratified turbulent flows have been incorporated into a closure model directly; then a one-dimensional version has been used to model the oceanic mixed layer [Galperin *et al.*, 1989]. In another approach, the turbulence model used in mixed layers has been somewhat simplified using the KE (turbulence kinetic energy approach), based on the specification of two 'master' length scales, one for dissipation and one for mixing [Gaspar *et al.*, 1990]. Their work was based on earlier successful use of such techniques in the atmospheric boundary layer [Bougeault and Lacarrere, 1989].

3.3. The Acoustic Models

Computer modeling of the acoustic field in the ocean is at present accomplished using a number of different model types. The diversity of models stems from the need to efficiently cover low to high frequencies, range-independent and range-dependent environments, and acoustic vs. elastic bottom types. In general, the choice of a model involves trade-offs between accuracy, run time and ease of use. We shall discuss briefly these different approximations and refer the reader to

Jensen *et al.* [1993] for a more complete discussion.

A useful starting point for underwater acoustics problems is the Helmholtz equation (or reduced wave equation). In two dimensions it reads as follows

$$\nabla^2 p + \frac{\omega^2}{c^2(r,z)} p = \frac{-\delta(r-r_s)\delta(z-z_s)}{r}, \tag{3.5}$$

where $c(r,z)$ is the ocean sound speed as a function of range and depth. In addition, ω is the angular frequency of the source which is located at the range/depth coordinate (r_s, z_s). The objective is to solve for the response of the channel to the source, that is to solve for the acoustic pressure $p(r,z)$. (The transmission loss (in dB) is then defined as $-20\log_{10}(4\pi|p(r,z)|)$.)

In principle it is straightforward to solve such an equation using, for instance, standard finite difference techniques. In practice, this is almost never done. The finite difference schemes require 6-10 points per wavelength so that a modest problem of 50 km in range and 5 km in depth would require a grid of around 10^6 points for a 10 Hz source. By present-day computer standards this problem is completely intractable.

For this reason a number of approximations have been introduced leading to principally four different kinds of models: 1) ray tracing, 2) spectral integral (Fast-Field Program), 3) normal mode, and 4) PE (parabolic equation). In the following sections we will briefly describe each of these approaches in terms of both their mathematical basis and domain of applicability.

3.3.1. Ray Theory

Ray-based models have been used for many years in underwater acoustics. In the early 60s virtually all modeling was done using either normal modes or ray tracing and primarily the latter. Today, however, ray tracing codes seem to have fallen somewhat out of favor in the research community, the problem being that the inherent (high-frequency) approximation of the method leads to somewhat coarse accuracy in the results. On the other hand, ray methods still enjoy a strong following in the operational environment where run-time is a critical factor, and environmental uncertainty poses much more severe constraints on the attainable accuracy.

To obtain the ray equations, one seeks a solution of the Helmholtz equation of the following form:

$$p(r,z) = e^{ik\phi(r,z)} \sum_{j=1}^{\infty} A_j(r,z) \frac{1}{(ik)^j}, \tag{3.6}$$

where $k = \omega/c_0$ and c_0 is a reference sound speed. Substituting into the Helmholtz equation one obtains an infinite sequence of equations for the functions $\phi(r,z)$ and $A_j(r,z)$:

$$(\nabla\phi)^2 = -c_0^2/c^2(r,z), \tag{3.7}$$

$$2\nabla\phi\cdot\nabla A_0 + (\Delta\phi)A_0 = 0, \tag{3.8}$$

$$2\nabla\phi\cdot\nabla A_j + (\Delta\phi)A_j = -\Delta A_{j-1}, \qquad j = 1,2,\ldots. \tag{3.9}$$

The equation for $\phi(r,z)$ is known as the *eikonal* equation while the equations for A_j are known as the *transport* equations. The eikonal equation is solved by introducing a family of curves (rays) which are defined by being perpendicular to the level curves (wavefronts) of $\phi(r,z)$. One finds that the rays satisfy:

$$\frac{dr}{ds} = c\rho(s), \qquad \frac{d\rho}{ds} = -\frac{1}{c^2}\frac{dc}{dr}, \tag{3.10}$$

$$\frac{dz}{ds} = c\zeta(s), \qquad \frac{d\zeta}{ds} = -\frac{1}{c^2}\frac{dc}{dz}, \tag{3.11}$$

where $(r(s), z(s))$ is the trajectory of the ray in the range-depth plane and $(\rho(s), \zeta(s))$ is the local tangent vector to the ray. Along such a ray, the phase function $\phi(r,z)$ is given by a simple integral:

$$\phi(s) = \int_0^s \frac{c_0}{c(s')}\, ds'. \tag{3.12}$$

In addition, it turns out that $A_0(r,z)$ also satisfies a simple differential equation along the ray. In essence, this equation states that the amplitude decays in proportion to the cross section of a ray tube. Higher order terms in the sequence $A_j(r,z)$ are generally not calculated in ray codes. Neglecting these terms is justified when the frequency is sufficiently high, since for large k the remaining terms $A_j/(ik)^j$ in Eq. (3.6) go to zero. Unfortunately, it is difficult to predict *a priori* what constitutes a "sufficiently high" frequency.

Despite this shortcoming, ray models remain an important class of models. In many cases their reduced accuracy compared to other models is irrelevant, since greater errors can easily be introduced by environmental uncertainty. Furthermore, for high-frequency or broadband problems the alternative models may simply require too much computer time. For this reason interest continues in improved or extended ray theories.

3.3.2. Spectral Integral Methods (Fast-Field Program)

The assumption that the environment is range independent or stratified leads to a great simplification of the governing equations. In essence the dimension of the problem is reduced by one. Starting with the Helmholtz equation given in Eq. (3.5), one applies a Fourier-Bessel transform:

$$\hat{p}(k,z) = \int_0^\infty p(r,z) J_0(kr) r\, dr, \tag{3.13}$$

which leads to:

$$\frac{d^2\hat{p}}{dz^2} + \left(\frac{\omega^2}{c^2(z)} - k^2\right)\hat{p} = \delta(z-z_s),$$

$$\hat{p}(0) = 0, \qquad \frac{d\hat{p}}{dz}(D) = 0, \tag{3.14}$$

where for simplicity we have used a pressure release surface boundary condition and a perfectly rigid bottom boundary condition at the depth $z = D$. The

solution of this boundary value problem yields $\hat{p}(k,z)$, and the final pressure is then computed using the inverse Fourier-Bessel transform as

$$p(r,z) = \int_0^\infty \hat{p}(k,z) J_0(kr) k \, dk. \tag{3.15}$$

This is the so-called spectral integral representation of the solution.

One can show that the kernel, $\hat{p}(k,z)$, decays rapidly to zero for $k > K$ where $K = \max(\omega/c(z))$. Thus, the integral need only be performed over the truncated interval $[0, K]$. However, the calculation of $p(r,z)$ requires the evaluation of this integral for every single point in range and depth of interest. Fortunately, a trick exists for performing these integrals efficiently. One uses the asymptotic approximation to the Bessel function to obtain,

$$p(r,z) \approx \frac{e^{i\pi/4}}{\sqrt{2\pi r}} \int_0^K \hat{p}(k,z) e^{ikr} \sqrt{k} \, dk. \tag{3.16}$$

This has the form of a Fourier transform and can be efficiently evaluated by an FFT.

In summary, the procedure is to solve Eq. (3.14) for a number of equally spaced k values to obtain a Green's function, $\hat{p}(k,z)$. This discretely sampled Green's function is then transformed using a FFT to obtain the acoustic pressure versus range.

Methods based on the spectral integral representation have been around for many years. The Fast Field Program (FFP) approach, distinguished by its use of the FFT to calculate the integral was originally suggested by Marsh and extended by DiNapoli (see DiNapoli and Deavenport [1980]) in the early 70s. Today there are several implementations of FFP codes with numerous extensions over the "bare-bones" model described above (see for instance, Schmidt and Jensen [1988]). This includes the capability of handling elastic media, interfacial roughness and impulsive sources.

In contrast to the ray solution, the FFP model yields a result which is essentially exact. Starting from the Helmholtz equation for a stratified medium, the only additional approximation is that of using the asymptotic approximation to the Bessel function. This approximation turns out to induce negligible errors beyond a wavelength or so from the source.

3.3.3. Normal Modes

Normal mode methods have been widely used for years in underwater acoustics. An early reference, that is widely cited is due to Pekeris [1948] who developed the theory for a simple two-layer model of the ocean. Today there are literally dozens of normal mode codes which allow the ocean sound speed profile to be included and in some cases also viscoelastic effects in the ocean subbottom.

The derivation of the governing equations is straightforward. Again one begins with the Helmholtz equation and seeks a solution as a sum of normal modes:

$$p(r,z) = \sum_{j=1}^{\infty} Z_j(z) R_j(r). \tag{3.17}$$

Substituting the above form into the Helmholtz equation one obtains:

$$\frac{d^2 Z_j}{dz^2} + \left(\frac{\omega^2}{c^2(z)} - k_j^2 \right) Z_j = 0,$$
$$Z_j(0) = 0, \qquad \frac{dZ_j}{dz}(D) = 0, \tag{3.18}$$

which is identical to the spectral integral form of Eq. (3.14) apart from lacking the forcing term on the right-hand side. The above equation has an infinite number of solutions which are like modes of a vibrating string. The modes are characterized by a mode shape function $Z_j(z)$ and a horizontal propagation constant k_j (analogous to a frequency of vibration).

The range functions, $R_j(r)$, are found to satisfy,

$$\frac{1}{r} \frac{\partial}{\partial r} \left(r \frac{\partial R_j}{\partial r} \right) + k_j^2 R_j = -Z_j(z_s) \frac{\delta(r)}{r}, \tag{3.19}$$

which has the solution $R_j(r) = \frac{i}{4} Z_j(z_s) H_0^{(1)}(k_j r)$. Putting this all together, one finds that,

$$p(r,z) = \frac{i}{4} \sum_{j=1}^{\infty} Z_j(z_s) Z_j(z) H_0^{(1)}(k_j r), \tag{3.20}$$

or, using the asymptotic approximation to the Hankel function,

$$p(r,z) \approx \frac{i}{\sqrt{8\pi r}} e^{-i\pi/4} \sum_{j=1}^{\infty} Z_j(z_s) Z_j(z) \frac{e^{ik_j r}}{\sqrt{k_j}}. \tag{3.21}$$

The normal mode result is typically accurate for ranges greater than the first 10 water depths or so, a figure which depends on the number of modes that are included in the solution. In the near-field the FFP solution provides a more precise result, since the normal mode series is truncated and therefore neglects steep angle ray paths. The advantage of the normal mode approach is that the far-field solution can be calculated very efficiently. Basically, the cost of an FFP solution increases in proportion to range due to the need of sampling the kernel more finely for greater ranges. The opposite is true for a normal mode code: in the near-field more and more modes must be computed. Beyond some intermediate range, for example, typically 10 water depths, the normal mode solution becomes more efficient.

Normal mode models tend to be thought of as providing solutions to range-independent problems. In fact, range-dependent (and even three-dimensional) solutions can also be provided using either (a) *adiabatic mode theory* or (b) *coupled mode theory*. (These extensions are discussed in the paper by Kuperman *et al.* in Chapter 7 of this volume). The latter approach requires more computer time but can provide more accurate answers.

3.3.4. Parabolic Equation Modeling

The parabolic equation was introduced in underwater acoustics in 1973 by Tappert and Hardin. One begins by seeking a solution of the Helmholtz equation in the form,

$$p(r,z) = u(r,z)H_0^{(1)}(k_0 r), \tag{3.22}$$

where k_0 is a reference wavenumber. Substituting into Eq. (3.5) one finds,

$$u_{rr} + 2ik_0 u_r + k_0^2(n^2-1)u + u_{zz} = 0. \tag{3.23}$$

At this point, one discards the first term to obtain the parabolic equation:

$$u_r = ik_0\frac{n^2-1}{2}u + \frac{i}{2k_0}u_{zz}. \tag{3.24}$$

This latter step is justified assuming weak range-dependence and narrow angle propagation, i.e., when the dominant energy comes from rays propagating nearly horizontally.

The advantage of the parabolic equation over the original Helmholtz equation is that the PE can be solved by a straightforward marching in range which requires much less computational effort. From a numerical point of view, this range marching is typically implemented using either standard finite difference techniques [Lee *et al.*, 1981] or using a fast Fourier transform as in the so-called 'split-step' method [Tappert, 1977].

In problems with strong range-dependence the PE method is generally the method of choice. The PE method however has several approximations. These approximations introduce errors which increase as the corresponding ray angle increases. However, a great deal of work has been done in the last 10 years to construct higher-angle PE's so that now the angle limitation is seldom a problem. This increased accuracy generally comes at the expense of computer time.

3.4. Acoustic Modeling of Surface-Duct Propagation

3.4.1. Range-Independent Mixed Layer

We consider the synthesized profile plotted in Fig. 3.2. In the upper 110 m we have an isothermal mixed layer. As discussed above, the increasing pressure provides an increase in sound speed to the bottom of the mixed layer. Below the mixed layer and down to about 600 m is a thermocline in which the temperature decreases with depth. The sound speed correspondingly decreases. Finally, below the main thermocline is a deep isothermal layer in which the sound speed profile is predominantly affected by the increasing pressure with depth causing the sound speed to increase again. This leads to bowl-shaped sound speed profile which is characteristic of deep-water scenarios.

The mixed layer is primarily of interest for mid- to high-frequency problems (above about 300 Hz) since for lower frequencies the mixed layer is an ineffective

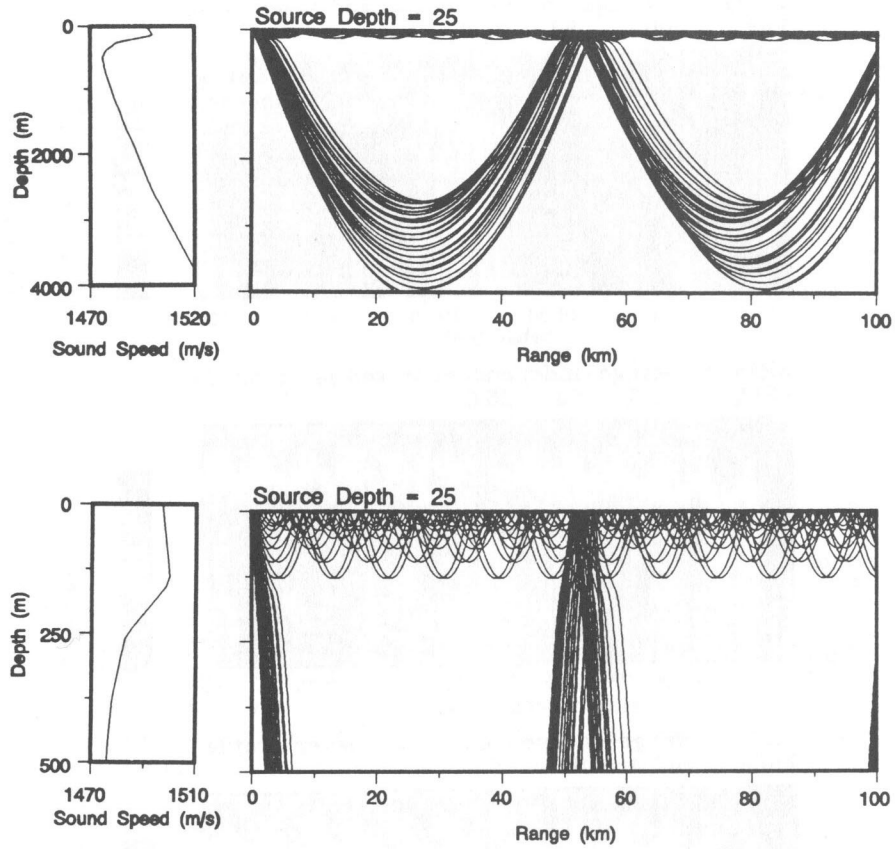

FIG. 3.2. Sound speed profile and ray trace for the range-independent problem, a) full-water column, b) enlargement of the upper 500 m.

acoustic duct. Considering high-frequency problems, it is natural to start with the ray-based approach.

For a source depth of 25 m, the ray trace shown in Fig. 3.2a manifests a fairly common deep-water "convergence zone" pattern in which rays cycle together in a band which refocuses at the surface approximately every 55 km. A blow-up of the upper 500 m shown in Fig. 3.2b highlights the effect of the surface duct: the locally upward refracting profile leads to ray paths which continually cycle toward the surface and reflect.

Transmission loss calculations using ray, normal mode, and split-step PE models (BELLHOP, KRAKEN, and PAREQ, respectively) are shown in Fig. 3.3. The normal mode result in Fig. 3.3b should be taken as the reference solution since the problem is range-independent. (The spectral integral solution is omitted since it is practically identical to the normal mode result.)

Note that the ray result in Fig. 3.3a shows significant errors. In particular, the

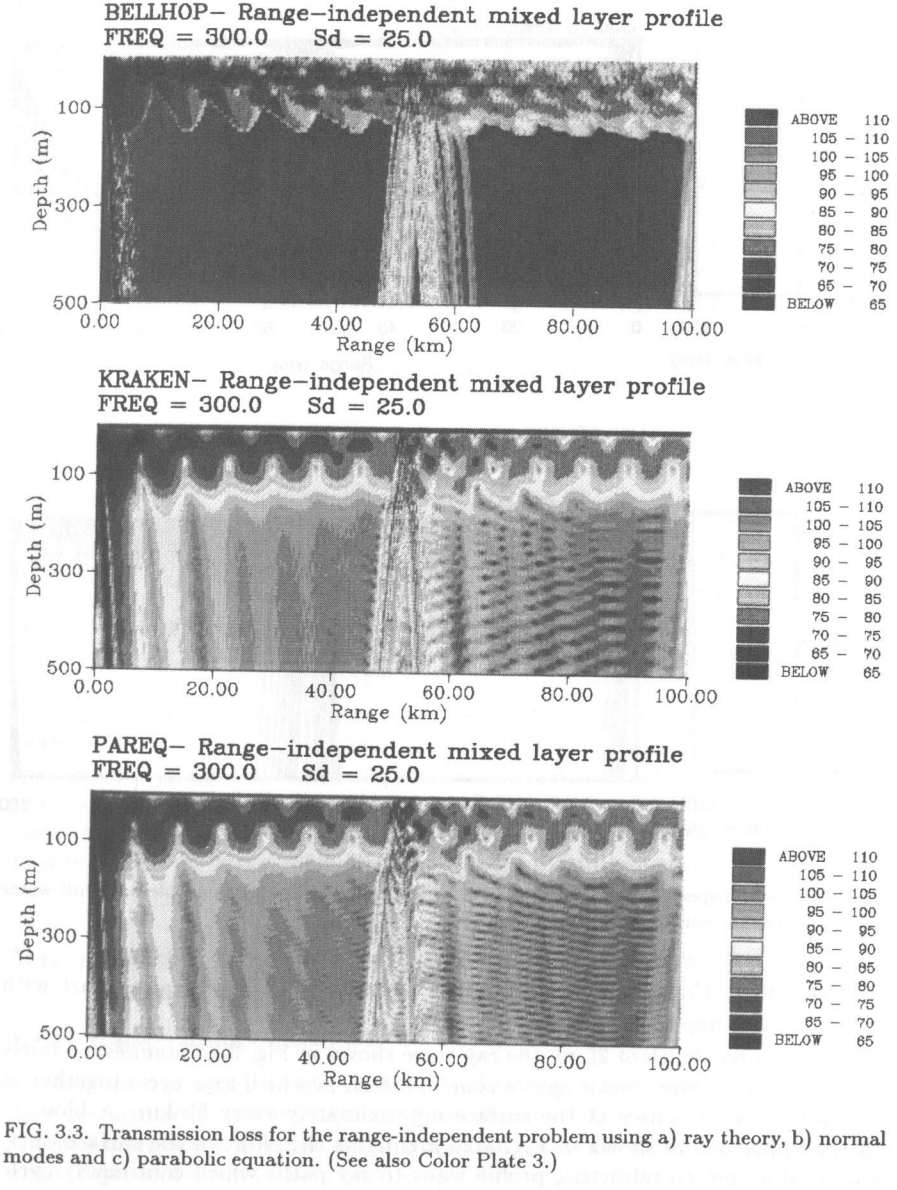

FIG. 3.3. Transmission loss for the range-independent problem using a) ray theory, b) normal modes and c) parabolic equation. (See also Color Plate 3.)

ray result manifests a perfect shadow below the surface duct while the normal mode result shows bands of high intensity which appear to be leaking out of the surface duct. If we focus just on the surface duct, we find that the ray model provides a good approximation to the mean levels but fails to reproduce the detailed structure of the intensity pattern.

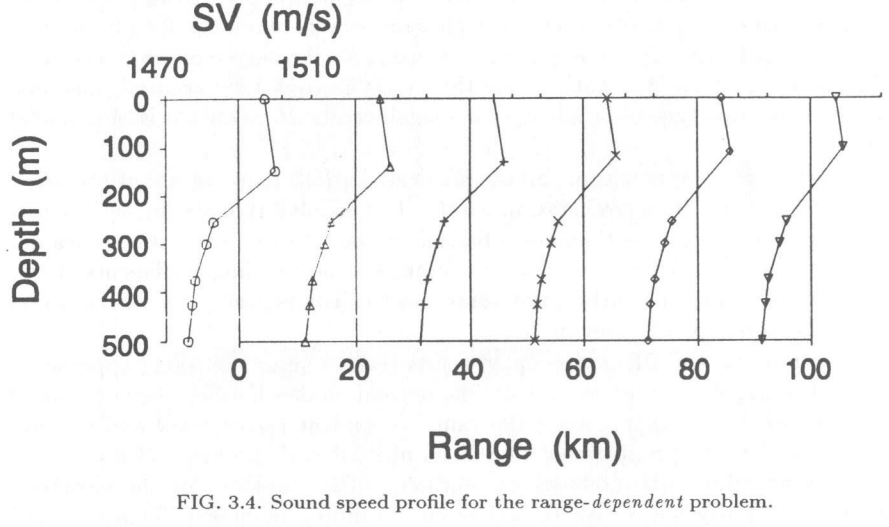

FIG. 3.4. Sound speed profile for the range-*dependent* problem.

As mentioned earlier, the ray approach is valid in the high-frequency limit but it is difficult to be quantitative about how low a frequency is acceptable. In part, there is simply a problem of deciding what threshold of accuracy is required which is in turn determined by operational considerations. However, even for a specified threshold it is difficult to say at what frequency the ray model will be valid. Loosely we can say that the wavelength must be small compared to *any* spatial scale in the problem. This includes the water depth, interior ducts, bathymetric features. In the case of this particular mixed-layer profile, the surface duct is clearly too small for accurate ray modeling.

The parabolic equation result in Fig. 3.3c requires several minor approximations which, judging from the excellent agreement with the normal mode result, are not significant. The run-times (VAXstation 3100) for these different models is as follows: ray tracing (7 minutes), normal mode (10 minutes), FFP (90 minutes) and PE (60 minutes).

3.4.2. Application to a Range-Dependent Mixed Layer

An idealized range-dependent scenario is illustrated in Fig. 3.4. The surface duct at the source is 150 m deep and gradually shoals to 100 m at a range of 100 km. As mentioned earlier, normal mode models have two common generalizations to range-dependent problems, namely adiabatic and coupled mode theory. The PE models are derived for range-dependent problems so no generalization is required.

The results of these three alternatives are shown in Fig. 3.5. Note that both the coupled mode (middle plot) and PE (lower plot) models provide similar answers. In this case, the approximations in both models are insignificant and so the results may be taken as reference solutions.

The effect of the narrowing of the surface duct is to reduce the trapping of acoustic energy and lead to lower levels within the duct. The adiabatic calculation shown in the Fig. 3.5a (top plot) shows a significant discrepancy with the PE and coupled mode solutions. The adiabatic approximation is valid in a limit of slow variation in range. Like the high-frequency requirement for ray models, it is difficult to give a precise quantitative value for the degree of range-variation that is acceptable. Adiabatic mode theory often gives very accurate answers; however, for this type of problem with a significant surface duct it is of doubtful utility.

In terms of computer time, all of these calculations required about the same time (60 minutes on a VAXstation 3100). The coupled mode solution is somewhat more cumbersome than the adiabatic mode solution, since it requires detailed sampling of the modes in order to compute the coupling coefficients. However, as we mentioned earlier, the adiabatic result is probably too coarse to be useful for this type of problem.

In summary, the PE and coupled mode codes remain as viable approaches for such range-dependent scenarios. The normal mode solutions were computed using 6 profiles to approximate the range-dependent mixed layer and the run times are directly proportional to the number of such profiles. (Each profile requires an additional mode-set calculation.) The run-time for the parabolic equation is fairly insensitive to the profile sampling in range. Thus, the PE solution is more attractive when finer profile sampling is required, for instance, in problems with strong bathymetric variation.

3.5. Sensitivity

Questions that arise frequently in oceanographic modeling are what parameters are most important and how accurately must they be known for acoustic modeling purposes. In order to address this question, we take a particular mixed-layer profile as a reference solution and examine changes (in transmission loss) which result as the mixed-layer profile is varied in particular ways. We consider here changes which yield range-independent profiles. As discussed above, a normal mode program is well-suited for such problems and is therefore employed for the various simulations.

The sound speed profile corresponding to our reference solution is shown in Fig. 3.6. The upper 500 m of the profile have been extracted from XBT measurements from the ocean weather ship, *Lima* and mated to climatological data for the remaining portion of the water column. The salinity was also taken from climatology. Next, transmission loss (TL) has been calculated using a normal mode program [Porter *et al.*, 1990] yielding the result shown in Fig. 3.7a. The frequency for this calculation is 600 Hz and the source depth is 25 m. As expected, the near-surface duct leads to trapping of acoustic energy in the upper 110 m. Note that transmission loss is plotted only in the upper 500 m of the water column.

In Fig. 3.7b we have modified the profile by increasing the mixed-layer sound speed by 12 m/s. In terms of mixed-layer temperature, this corresponds to a

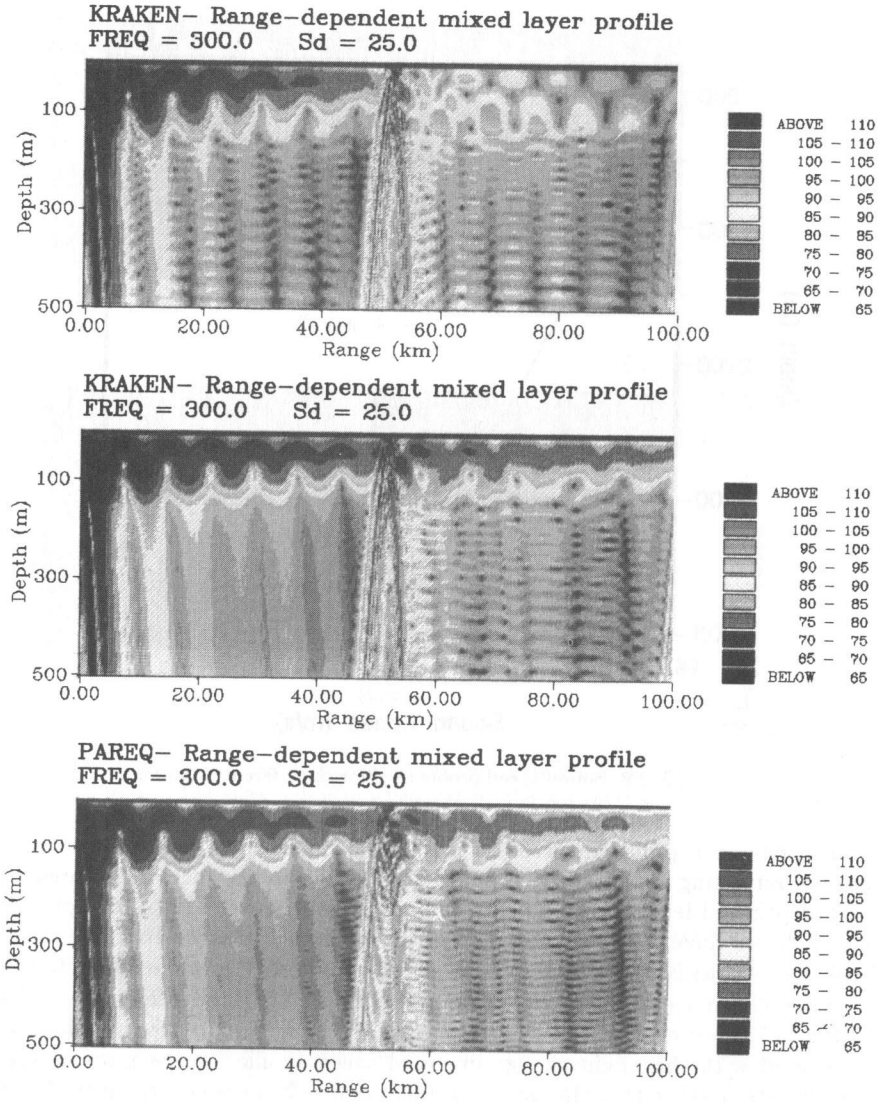

FIG. 3.5. Transmission loss for the range-dependent problem using a) adiabatic mode theory, b) coupled mode theory and c) PE. (See also Color Plate 4.)

temperature offset of about 3°C. Interestingly, there is *negligible change* in the transmission loss. The proposal has sometimes emerged of using satellite data to correct sea-surface temperature. An implication of this result is that an *a posteriori* correction is not very useful in terms of acoustic impact. (However, such information may be quite useful in providing forcing functions for mixed-layer models.)

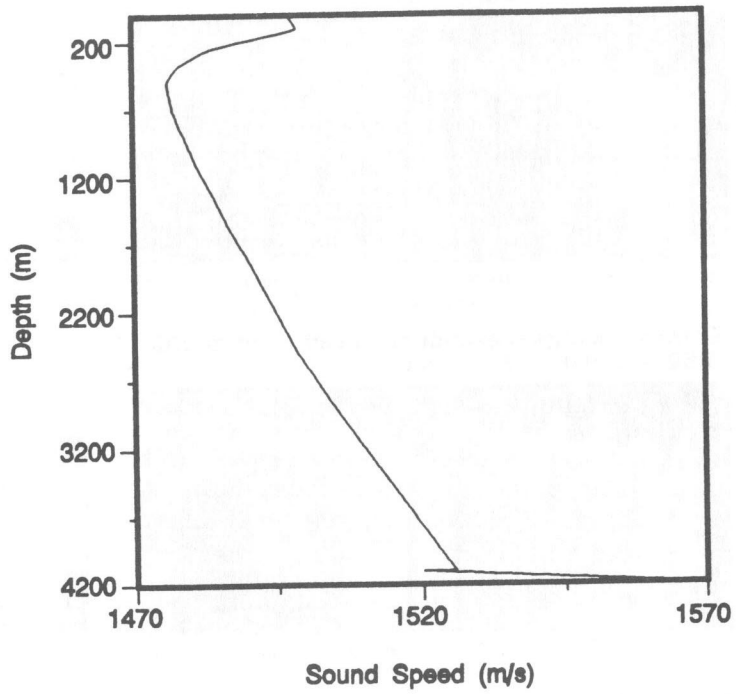

FIG. 3.6. Sound speed profile used for the reference solution.

The reference profile involves an isothermal mixed layer which leads to an *upward* refracting sound speed profile. This is due to the increase in pressure with depth and leads to a gradient of about 1.75 m/s over 110 m in depth. In Fig. 3.8a we have changed the gradient in the mixed layer so that the mixed layer has a *downward* refracting sound speed profile with a gradient -1.75 m/s over the 110 m deep mixed layer. Comparing Fig. 3.8a to the reference solution in Fig. 3.7a, we see that there is a tremendous change in the transmission loss associated with this slight change in sound speed profile. To be more precise, the acoustic level within the duct is greatly reducedp however, receivers below the duct see very little change.

Finally, in Fig. 3.8b we demonstrate the effect of changing the mixed layer depth. The reference solution involves a mixed layer of 110 m in depth while the perturbed solution has a mixed layer of 55 m in depth. We observe that for our 600 Hz source frequency the 55 m duct is much less effective at trapping energy. The transition from ducting to nonducting is somewhat nebulous; however, as discussed in Urick [1983], the formula $f = 1500/(0.008\,\mathrm{H}^{3/2})$ gives a reasonable estimate of the lowest frequency, f, for which energy will be trapped in a duct of height, H (in units of meters). (This formula assumes an isothermal mixed layer.) Thus, for our 55 m mixed-layer "significant" ducting would occur for a

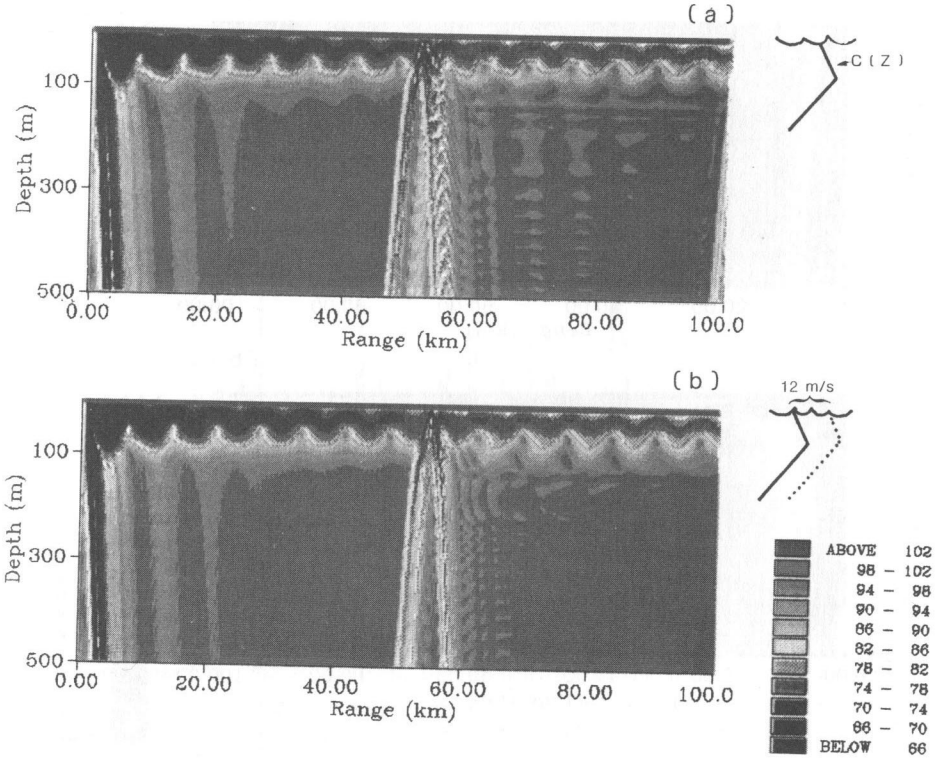

FIG. 3.7. Transmission loss calculations for a) reference profile and b) profile with mixed-layer offset by 12 m/s. (The inset indicates schematically the difference between the perturbed profile (dotted) and reference profile (solid).) (See also Color Plate 5.)

frequency of about 500 Hz.

One would like to derive from these kinds of results some general rule such as "mixed-layer depth must be known to ± 10 m." This, however, involves judgments which are somewhat subjective. Consider for instance a receiver located just below the *predicted* mixed layer, e.g., at a depth of 70 m in Fig. 3.8b. In this case, the receiver is in the shadow zone and the acoustic model predicts very high transmission loss. If the actual mixed-layer depth is 100 m, then such a receiver would be inside the duct and flooded by surface duct energy. On the other hand, if the source or receiver depth is uncertain by 20 m, then this may easily be the dominant source of error.

The above examples have been selected from a more complete parameter study to indicate the most important features. We mention in passing a few other points which emerged from this study. First, there are particular cases when a small change in mixed-layer temperature can make a big change in the resulting TL. For instance, this occurs when the duct is weak and the temperature change causes a transition between bottom limited (no depth excess) and non-bottom-limited (depth excess) propagation. Thus, a small change in ML temperature

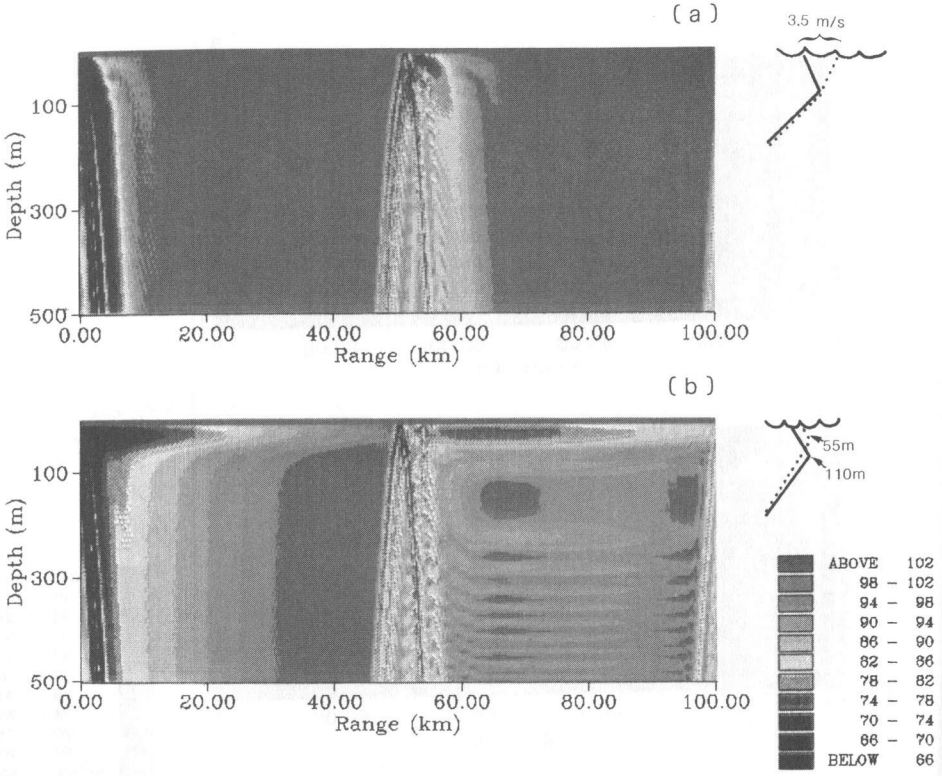

FIG. 3.8. Transmission loss calculations for a) profile with mixed-layer gradient changed to −.016/s and b) to 55 m. (The inset indicates schematically the difference between the perturbed profile (dotted) and reference profile (solid).) (See also Color Plate 6.)

can destroy all convergence zone paths.

Second, we have examined the role of surface scatter. Mixed-layer effects like surface scatter become more conspicuous as frequency increases. Errors in TL are associated with errors in predicting the surface scatter as well as errors in the ML predictions; if one dominates, it should be considered preferentially. We find that for the particular scenarios described above, surface scatter due to RMS roughness of 0.5 m plays a negligible role in the TL. At higher frequencies (3.5 kHz) surface scatter is extremely important. (Roughly, surface scatter loss varies as the square of frequency times surface roughness.)

Obviously, errors in mixed-layer predictions are not limited to the three parameters of temperature offset, gradient and mixed-layer depth. Nevertheless, an understanding of the sensitivity to these three basic parameters provides some useful insights. It is interesting that mixed-layer depth has become a fairly standard measure for comparing various models, yet it turns out that mixed-layer gradient is actually a much more important parameter in terms of acoustic predictions. Unfortunately, for mixed layers which are not strictly linear in sound speed profile the gradient is poorly defined. We could define a mixed-layer

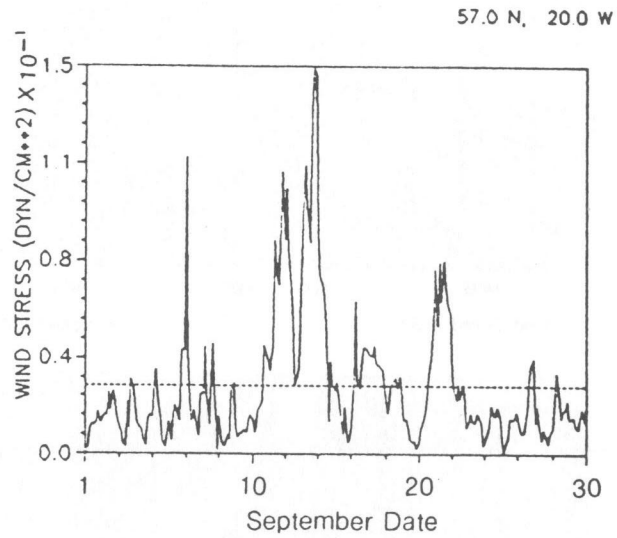

FIG. 3.9. Wind stress at weather ship Lima during September of 1985.

gradient based on the slope from top to bottom of the mixed layer; however, for profiles which vary nonlinearly with depth this is not a useful measure of ducting. Thus, it is difficult to recommend a single parameter for characterizing the accuracy of a mixed-layer model.

3.6. Mixed-Layer Models vs. Data

The results of the above sensitivity study will now be considered in more concrete terms by using actual mixed-layer model output. Ground truth for the following simulations comes from XBT measurements made by ocean weather ship *Lima* (57N, 20W) in September of 1985. The XBT profile measured on September 5 was used to initialize the Niiler mixed-layer model [Niiler, 1975]. Forcing terms such as the local wind and solar flux were also measured by the weather ship. Of particular interest is the wind stress which is plotted in Fig. 3.9 and shows the development of strong winds on approximately Sept. 10 and lasting for several days. The effect of these winds is to provide a substantial deepening of the mixed layer which is clearly manifest in the plots of the experimentally measured sound speed profile in Fig. 3.10.

As may also be seen in Fig. 3.10, the Niiler mixed-layer model (MLM) provides a satisfactory tracking of this event. That is, by a conventional measure of mixed-layer depth, the model does extremely well in tracking the deepening of the mixed layer. However, as was demonstrated in the previous section, the gradient is a much more important parameter. Thus, we can anticipate where a TL calculation based on the MLM will differ greatly from one based on the

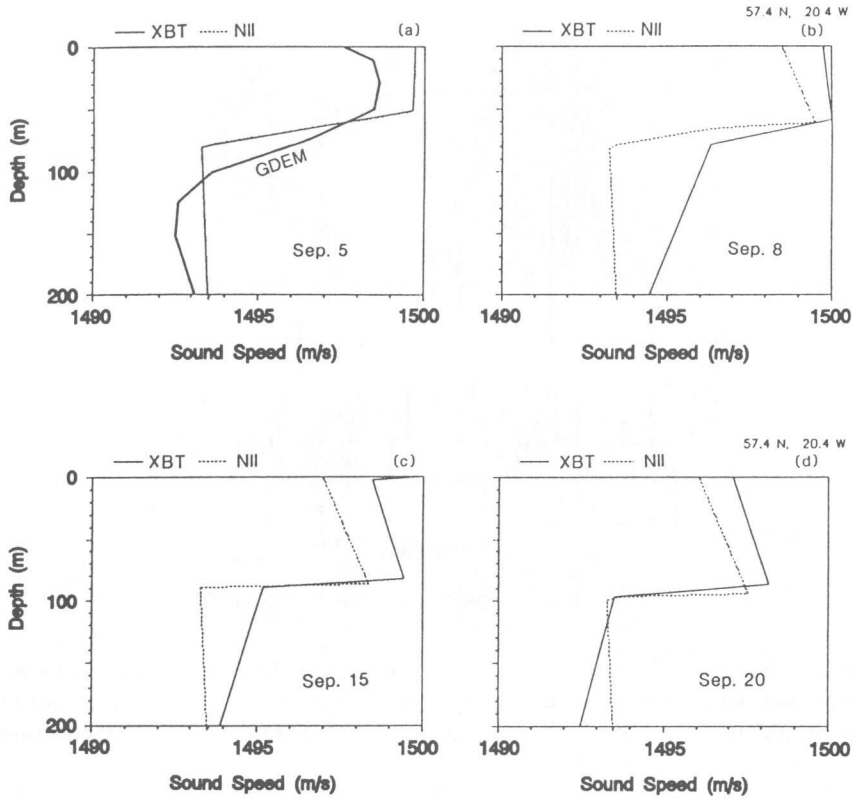

FIG. 3.10. Comparison of experimentally measured (solid line) and ML modeled (dashed line) sound speed profile. In (a) where the XBT and model profiles are identical, the summer GDEM profile (climatology) is also shown.

XBTs. On Sept. 8, we see that both the XBT and Niiler models show an upward-refracting mixed layer; however, the gradient in the XBT profile is much weaker. Thus, we anticipate poor agreement between the TL predictions. On the other hand, by Sept. 20, the model and data agree both in mixed-layer gradient and depth; however, the profile is offset. Considering our sensitivity study, we may anticipate a good agreement in the TL calculation.

These predictions are borne out in the actual transmission loss plots for these days shown in Figs. 3.11 and 3.12. (As before, the frequency is 600 Hz and the source depth is 25 m.) In both figures we see from top to bottom the TL results using sound speed profiles derived from XBT, MLM, and climatological data. The climatology is taken from the GDEM [Davis *et al.*, 1986] data base which provides temperature and salinity profiles on a seasonal basis from which the SSP was calculated. (The climatological SSP is also plotted in Fig. 3.11a.) The data from the weather ship is included in the database which implies this is a favorable location for climatology. A seasonal average, however, cannot hope

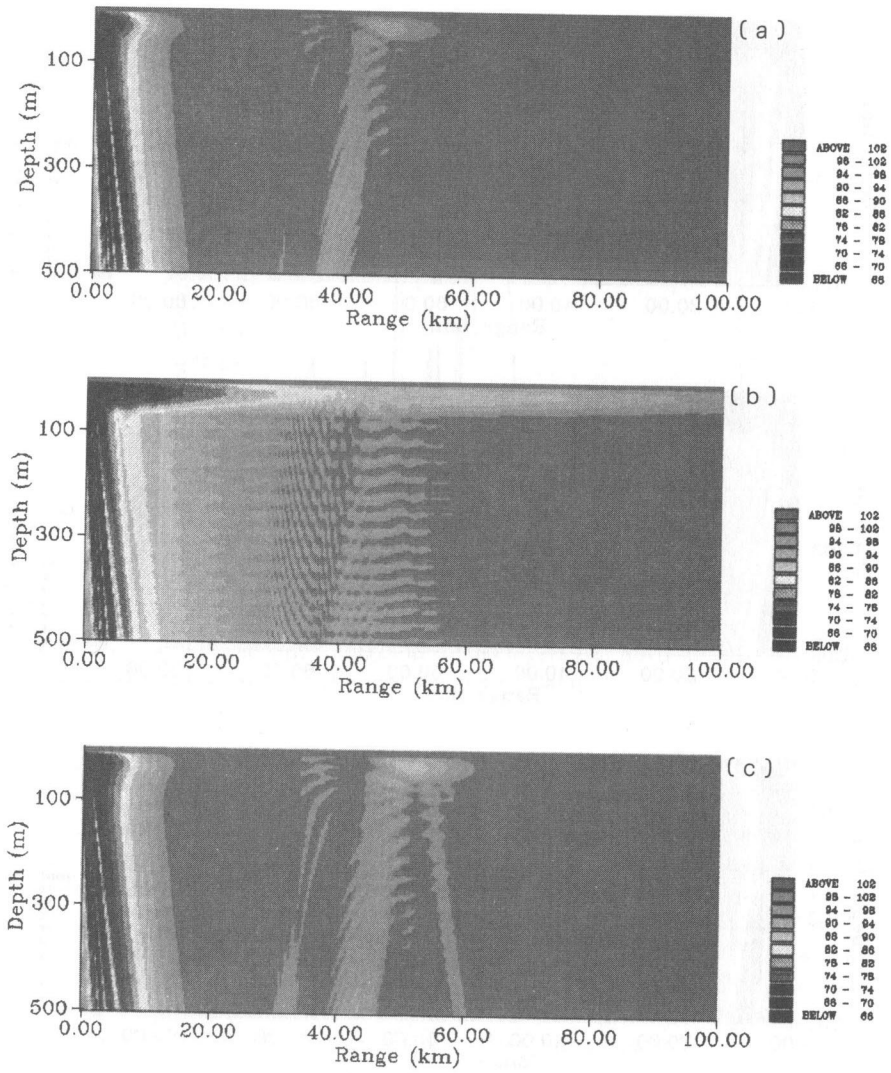

FIG. 3.11. Transmission loss on September 8 using a) experimental measurements, b) ML model and c) climatology for sound speed profile. (See also Color Plate 7.)

to provide much accuracy during a storm event. Thus, we see that climatology (Fig. 3.11c) agrees quite well with the XBT results (Fig. 3.11a) on Sept. 8. In fact the agreement with the XBT solution is actually better than the MLM, because of the incorrect gradient in the latter. However, by Sept. 20 the climatological profile bears little resemblance to the measured profile while the MLM does quite well.

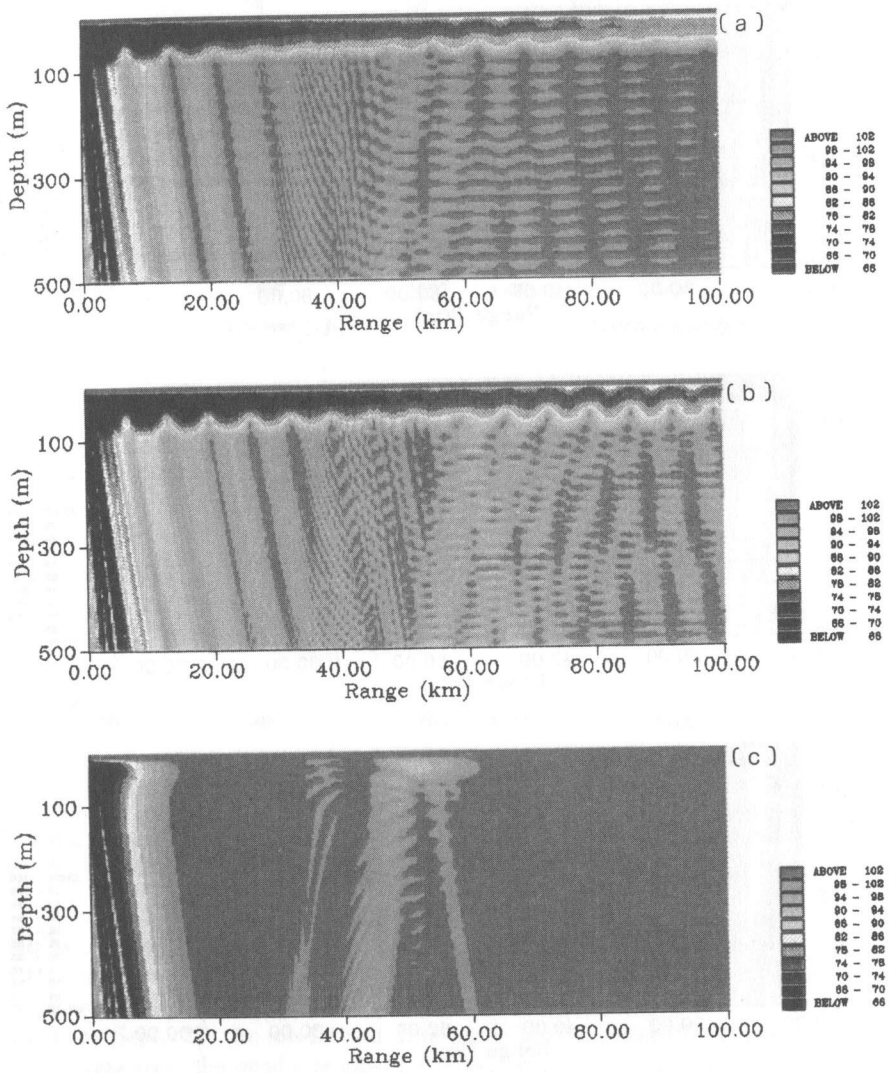

FIG. 3.12. Transmission loss on September 20 using a) experimental measurements, b) ML model and c) climatology for sound speed profile. (See also Color Plate 8.)

One cannot conclude from these results whether climatology is in general better or worse than the MLM and indeed this is not our objective. We must also caution that the XBT data is somewhat undersampled in depth so that the MLM profile may actually be providing a better answer than the XBT profile on Sept. 8. At any rate several points are illustrated by this comparison. First, mixed-layer depth is an inadequate criterion for judging the performance of a

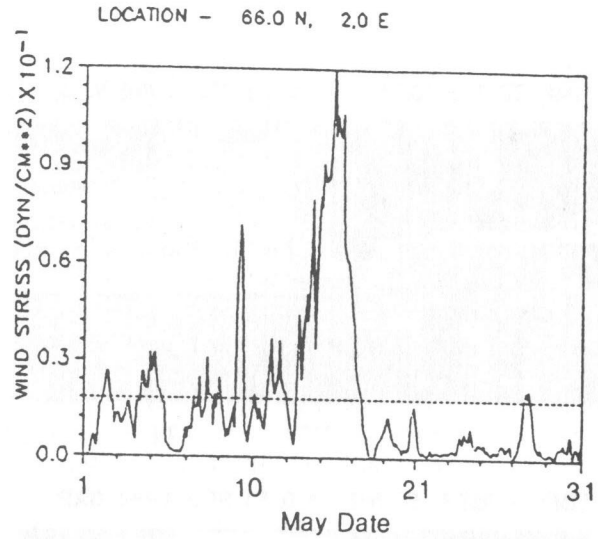

FIG. 3.13. Wind stress at weather ship *Mike* during May 1964.

mixed-layer model. Second, changes in mixed layers can have an important effect on transmission loss even in the mid-frequency band.

3.7. Mixed-Layer Model Comparison

Previous mixed-layer studies have shown that appreciable differences arise in the predicted SST (sea-surface temperature) and MLD (mixed-layer depth) if different models are used. Most of these experiments have been performed at weather ship sites Papa and November in the North Pacific [Martin, 1985], where a strong halocline prevents the formation of very deep mixed layers. Here we have tested these models in the Northeast Atlantic, in particular the GIN (Greenland-Iceland-Norwegian) Sea where much deeper mixed layers have been observed, with corresponding ducting effects at much lower frequencies.

To include both a cooling/deepening and a warming/shallowing event, we have chosen to simulate the mixed-layer development during May 1964, in the neighborhood of the weather ship *Mike*. The exact hydrographic location chosen is 62.5N, 1.0E, where the predominant water mass characteristics are typically those of the North Atlantic Inflow water, with a gentle decrease of temperature in the seasonal thermocline and, in the winter, deep mixed layers.

Figure 3.13 shows the wind forcing in May 1964, dominated by a rather large, somewhat unseasonable but by no means uncommon storm commencing on May 9 and ending around May 18. The remaining period in May is characterized by rather light winds which allow the seasonal warming to proceed almost uninhibited, providing only enough mixing to transport the heat downward to lower

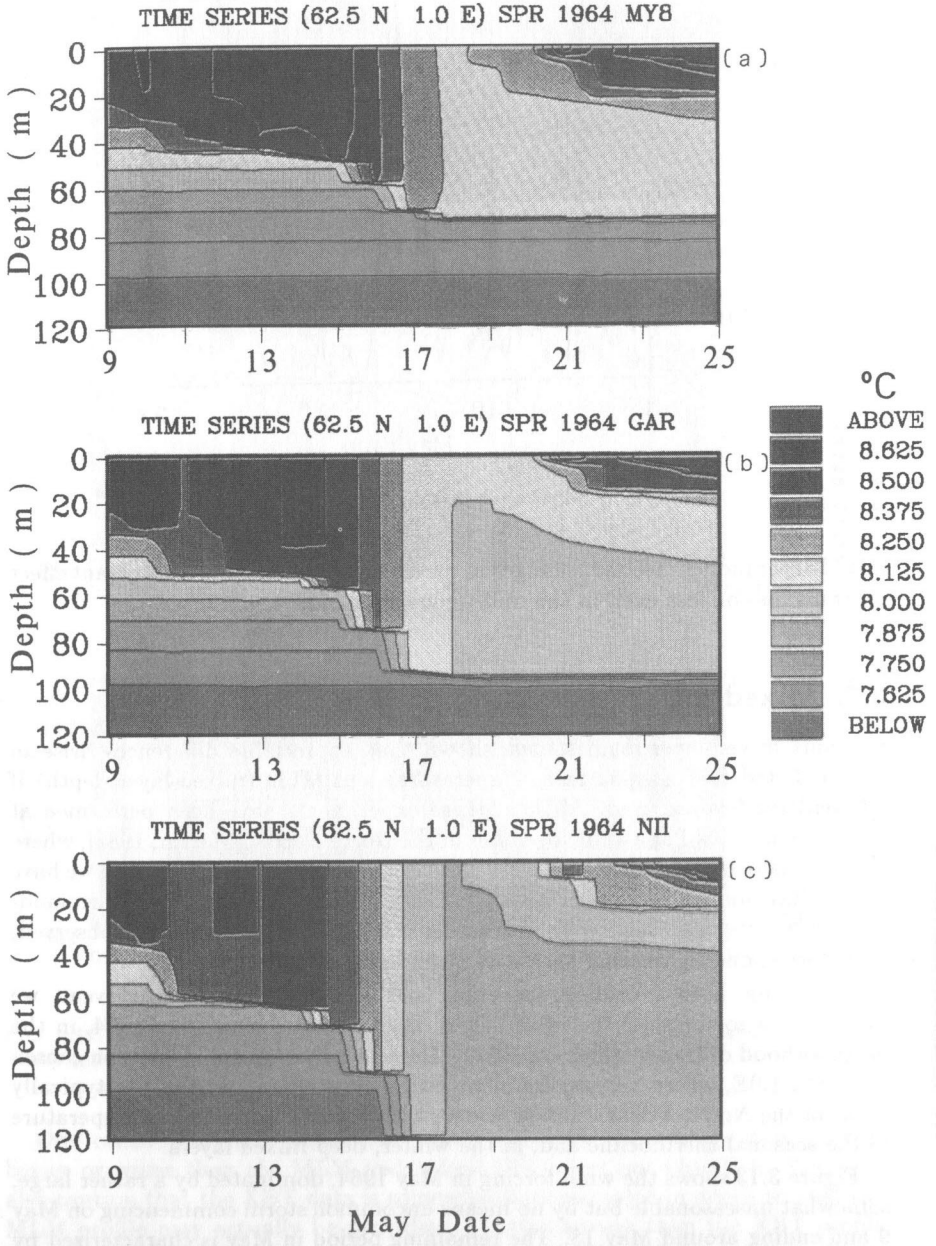

FIG. 3.14. Evolution of the mixed-layer temperature calculated using a) Mellor-Yamada Level 2.5, b) Garwood and c) Niiler models. (See also Color Plate 9.)

layers, thus preventing the formation of an excessively warm near-surface layer. The particular onset time of the heating was also influenced by the appearance of clear skies and a warmer overlying air mass.

The mixed-layer development over time is illustrated in Fig. 3.14, as obtained by three models: the Mellor-Yamada Level 2.5 (a "profile type"), the Garwood (a "bulk" type), and the Niiler (another "bulk" type). The general behavior of the model-predicted temperature field is the same for all models, but there are important quantitative differences. In all models, the mixed-layer deepening proceeds more or less steadily for the eight days of the storm, until about May 17; then the mixed layer becomes stationary. On about May 20, a marked surface heating episode commences and continues until the end of the month.

In Fig. 3.14 the results are presented in order of increasing mixing efficiencies: the MY2.5 mixing the least and the Niiler mixing the most. The MY2.5 model mixes to a final depth of about 75–80 m, the Garwood model to about 95–100 m, and the Niiler model to about 100–105 m. The total simulation region had a depth of 200 m, but only the top 120 m are presented here in order to further enhance variations within the mixed layer, and to better observe the transition region below it. In these discussions we would rather avoid giving an exact definition of mixed-layer depth (MLD), which can be based on the depth at which various physical quantities fall a certain increment below their surface value (e.g., 0.2°C for temperature), or at which they reach their near-surface maximum (e.g., sound speed, Brunt-Väisäla frequency). At any rate, when multiple well-mixed layers appear these definitions lead to ambiguities and are not very adequate, as for example during the heating period in the last 10 days of May. We will rather confine ourselves to simple *ad hoc* definitions and estimates that best describe the results presented in these figures. With this in mind, the contour intervals and shading scales have been selected to best present the regions of strong mixing and the transition region immediately below it, but neglecting the seasonal thermocline.

The depths of the new surface layers due to the late-May heating are again predicted in the same order, with the MY2.5 model predicting a depth of about 20 m, the Garwood model a depth of about 30 m, and the Niiler model about 40 m. A useful definition of the MLD here is the depth of the isotherm representing the first 0.2°C increase above the temperature of the storm-induced deep mixed layer.

The corresponding acoustic propagation results are illustrated in Fig. 3.15, for a frequency of 600 Hz and a source depth of 25 m. Figure 3.15a shows the propagation in the initial environment, taken from spring climatology. There is only a very shallow mixed-layer present initially, of about 10 m in depth, and there is no evidence of any duct for this frequency. Figures 3.15b,c show the propagation in the environment present at the end of the storm, on May 19, the eighth day of the simulation, as predicted by the MY2.5 and the Niiler models, respectively. We see that only a moderate "ducting" occurs in the MY2.5 environment, but a rather strong duct is present (for 600 Hz) in the Niiler environment. The results of the Garwood model (not shown) fall somewhere in-between.

Figure 3.16 presents the acoustic propagation results in the environments pre-

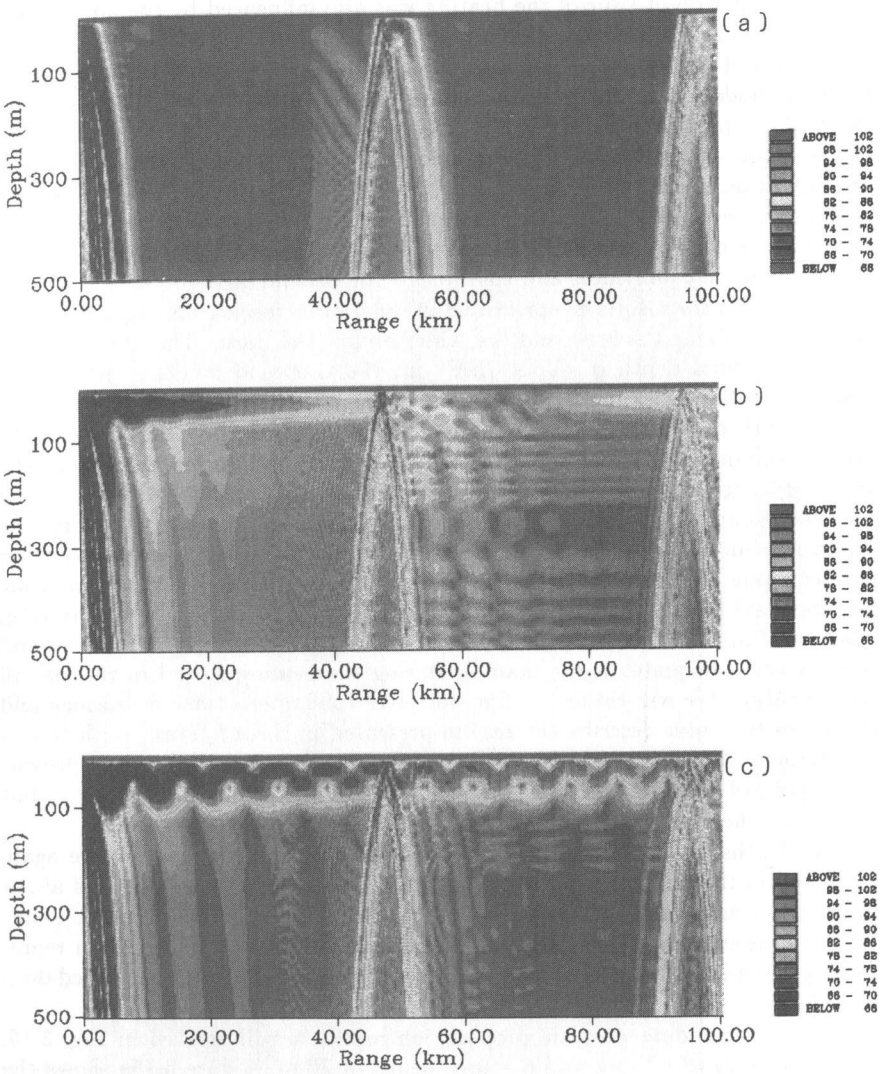

FIG. 3.15. Transmission loss on May 19 (day 8) using a) the climatology initial condition, b) Mellor-Yamada Level 2.5 MLM and c) Niiler MLM for the mixed-layer profile. (Plate 10.)

dicted for May 23, day 12 of the simulations, at the end of the heating period. The conclusions for the simulations of May 19 apply here, too, with significant ducting occurring only in the Niiler environment. In comparison to the previous figure, we observe that the surface heating has induced fairly minor changes in the TL plots. Both models show some increase in TL which is associated with a reduction in surface duct thickness. The differences between the individ-

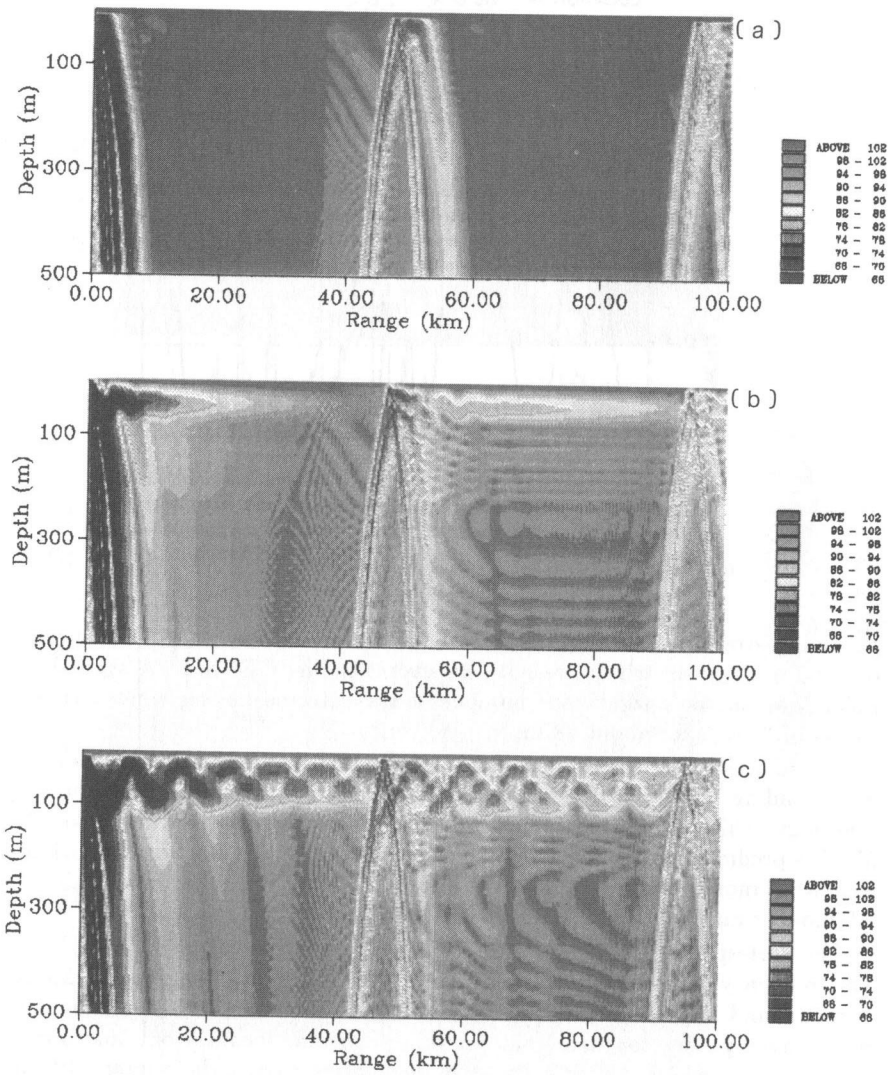

FIG. 3.16. Transmission loss on May 23 (day 12) using a) the climatology initial condition, b) Mellor-Yamada Level 2.5 MLM and c) Niiler MLM for the mixed-layer profile. (Plate 11.)

ual models are more important than the differences resulting from the surface heating.

To capture a very deep winter mixing event, with its potential ducting effect on even lower frequencies, we have simulated the mixed-layer behavior during the large winter storm of February 1960, commencing on February 3. The time history of the wind stress is illustrated in Fig. 3.17. Even this large storm,

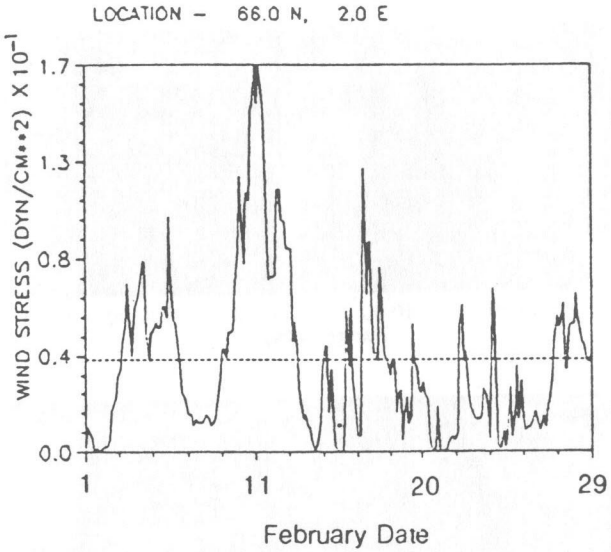

FIG. 3.17. Wind stress at weather ship Mike during February of 1960.

obtaining stress peaks of approximately 17 dynes, represents a wind speed of only 60 mph or so, which are not rare events in the GIN Sea. A statistics of polar lows shows a significant number of such storms having wind speeds in excess of 35 m/s, or about 78 mph.

Figure 3.18 shows the evolution of the mixed layer, commencing on February 3 and ending February 19. Again, the initial state was taken from winter climatology, which shows the typical mixed-layer depth to be 130 m or so. The MLD is predicted to deepen slowly to about 225 m by the Garwood model, and somewhat more rapidly to a depth of about 275 m by the Niiler model; the MY 2.5 model causes very little noticeable deepening.

The corresponding acoustic propagation results are illustrated in Fig. 3.19. The frequency has been reduced to 200 Hz, yet all three profiles (GDEM, Mellor-Yamada, and Niiler) show significant ducting. Taking the GDEM as a plausible winter average, we conclude that for this particular location one may expect significant mixed-layer effects for such frequencies during the winter. Placing some faith in the mixed-layer models we may anticipate that significant surface ducting will occur for frequencies as low as 50 Hz during certain times of the year.

3.8. Summary and Conclusions

We have presented a set of oceanic and acoustic simulation studies for the oceanic surface mixed layers found at high latitudes. The sensitivity study indicates that the near-surface temperature gradient (say in the upper 100 m), is an extremely

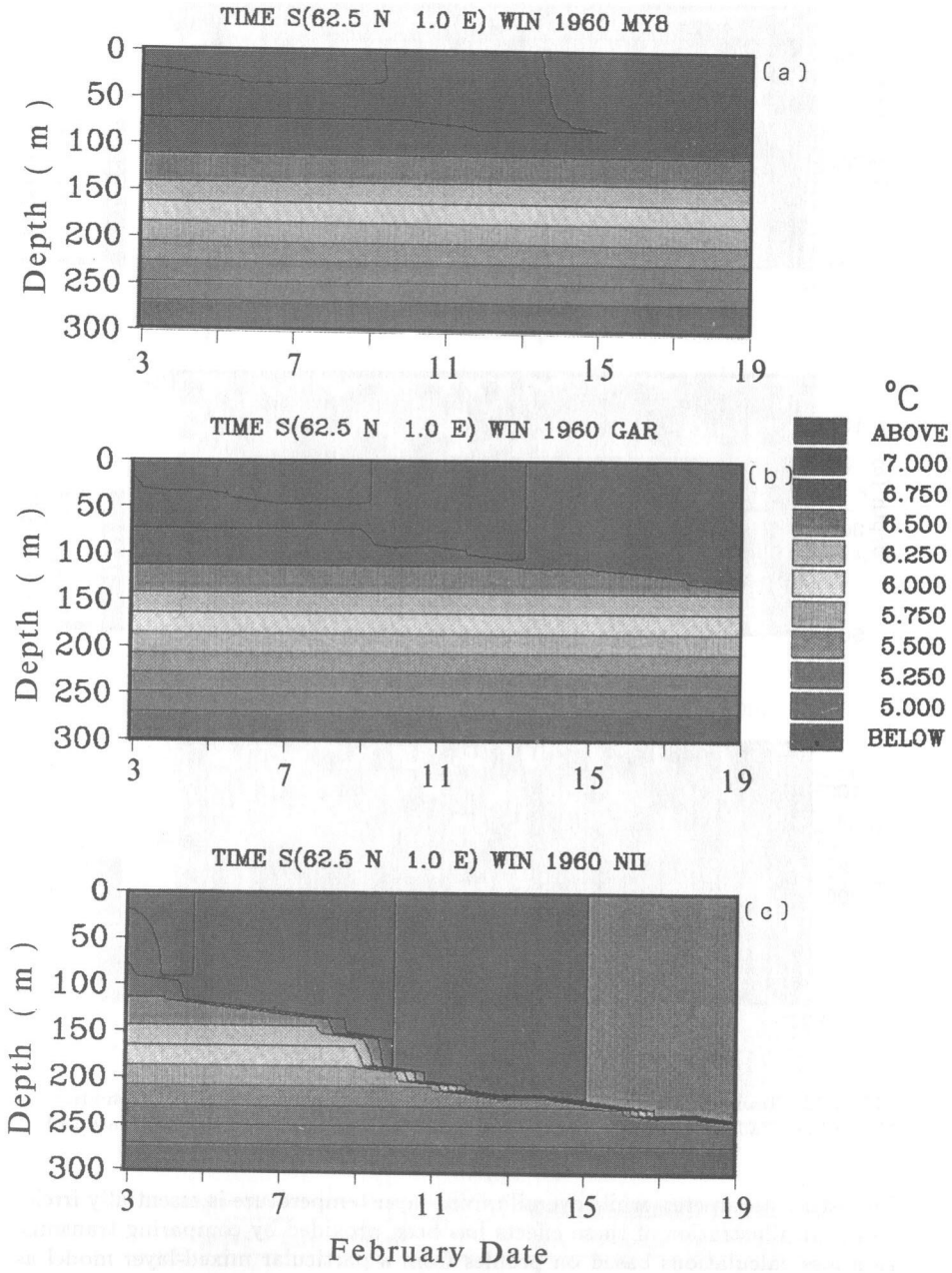

FIG. 3.18. Evolution of the mixed-layer temperature calculated using a) Mellor-Yamada Level 2.5, b) Garwood and c) Niiler models. (See also Color Plate 12.)

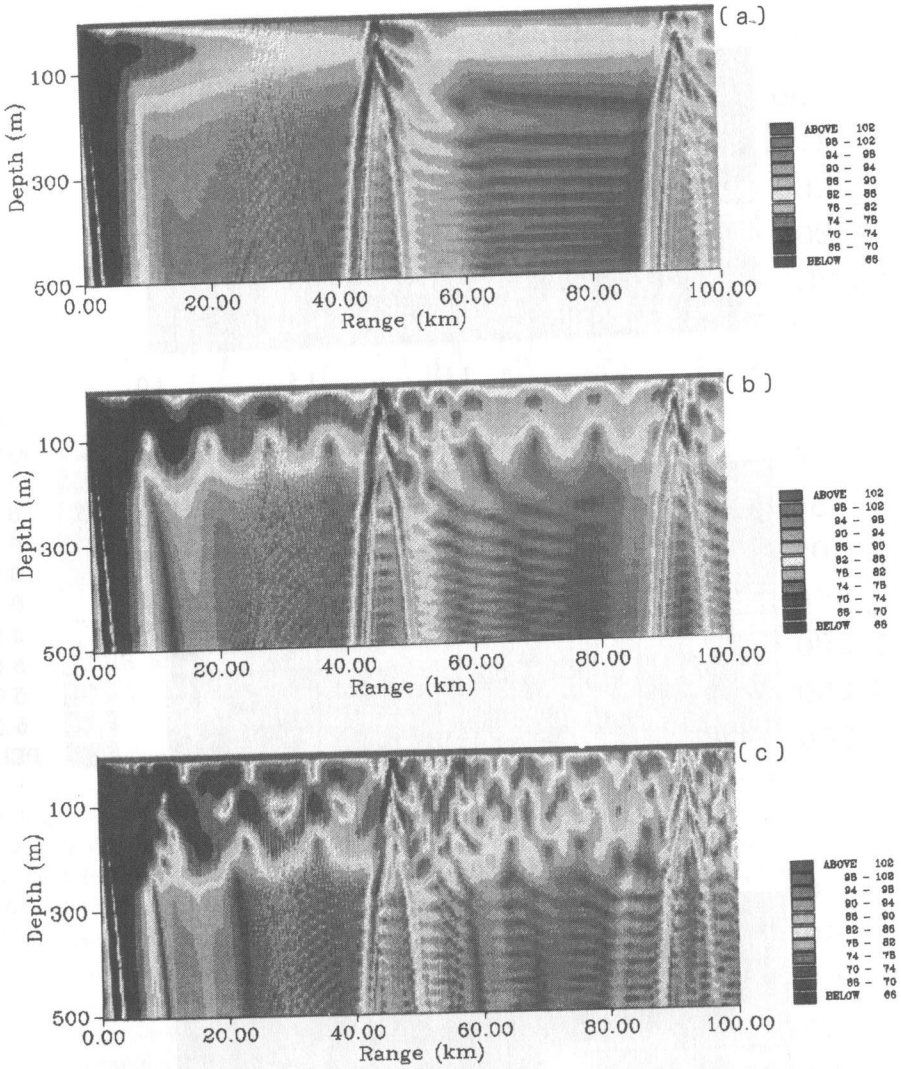

FIG. 3.19. Transmission loss on February 18 using a) the climatology initial condition, b) Mellor-Yamada Level 2.5 MLM and c) Niiler MLM for the mixed-layer profile. (Plate 13.)

important parameter, while overall mixed-layer temperature is essentially irrelevant. An illustration of these effects has been provided by comparing transmission loss calculations based on profiles from a particular mixed-layer model as well as measured and climatological profiles.

Comparisons of particular mixed-layer models have shown that the different models predict substantial differences in the mixed-layer depth. This in turn

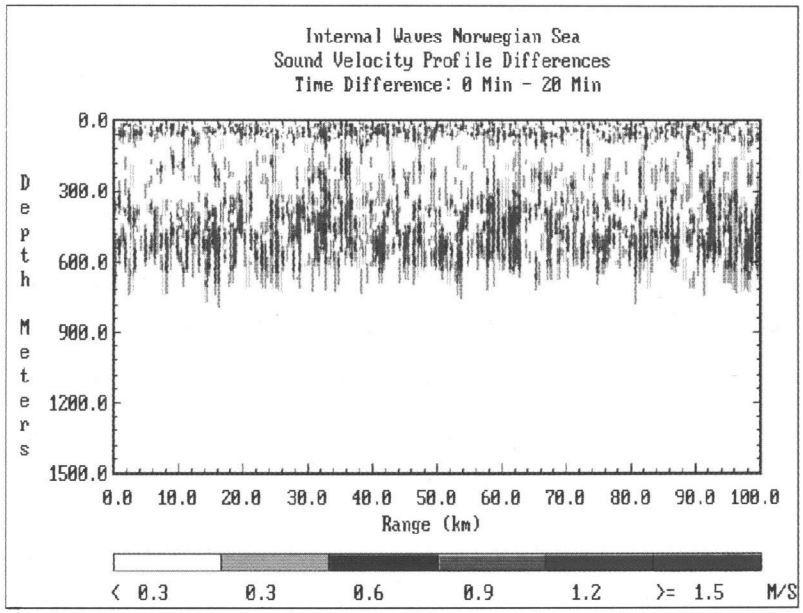

Plate 1. Differences between sound speeds in an internal wave region for time t=0 min and time t=20 min. (*Black and white version of figure available on p. 28.*)

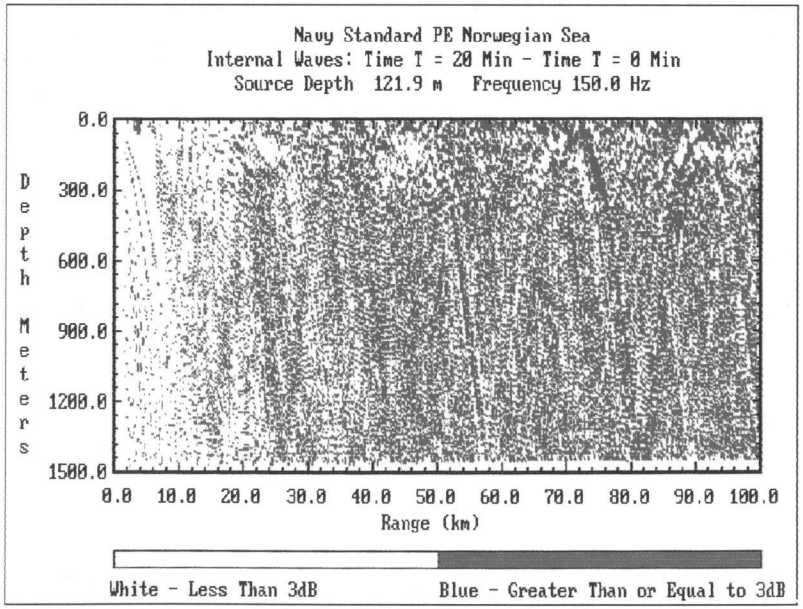

Plate 2. Differences between transmission loss (in dB) in an internal wave region for time t=0 min and time t=20 min. Dark areas are where the difference in transmission loss is equal to or greater than 3 dB. (*Black and white version of figure available on p. 30.*)

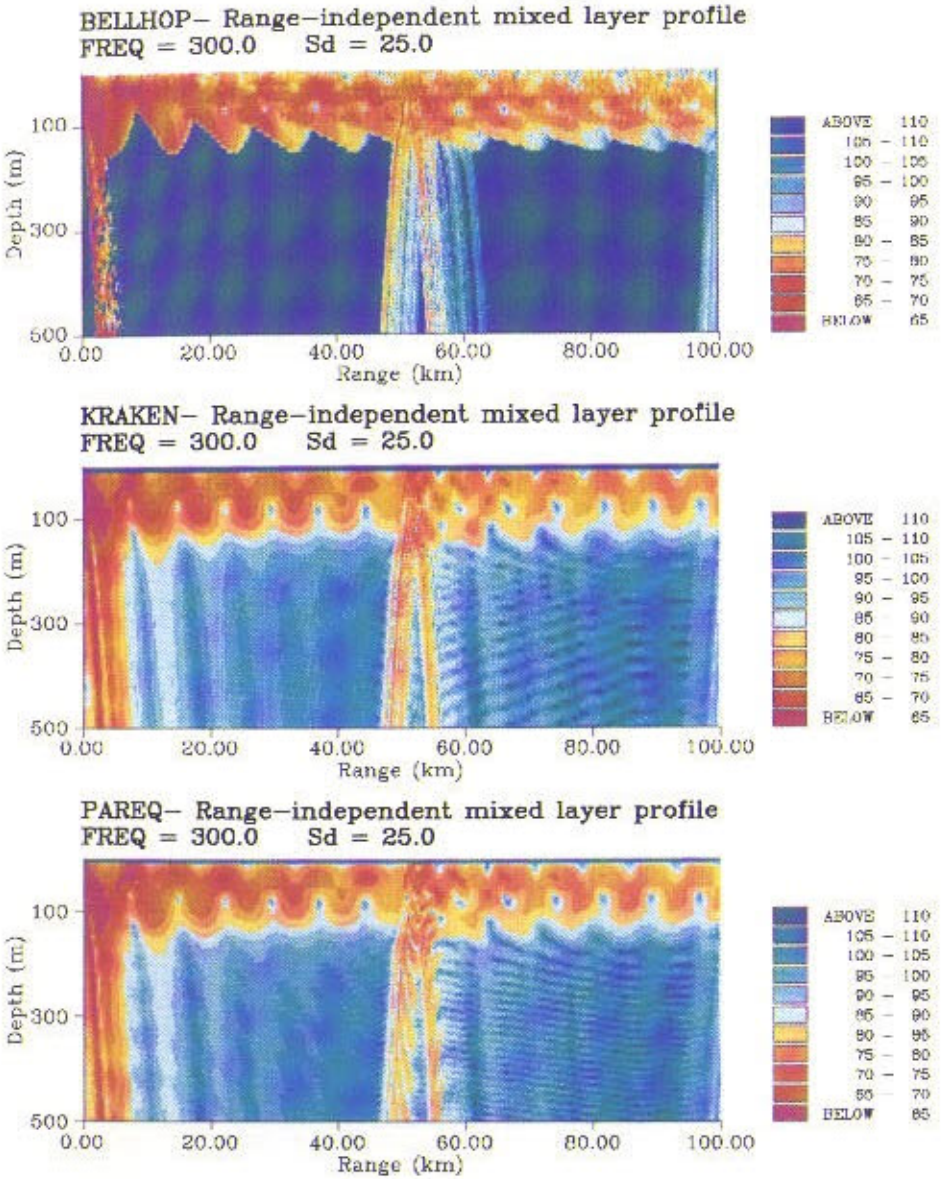

Plate 3. Transmission loss for the range-independent problem using **(a)** ray theory, **(b)** normal modes and **(c)** parabolic equation. *(Black and white version of figure available on p. 60.)*

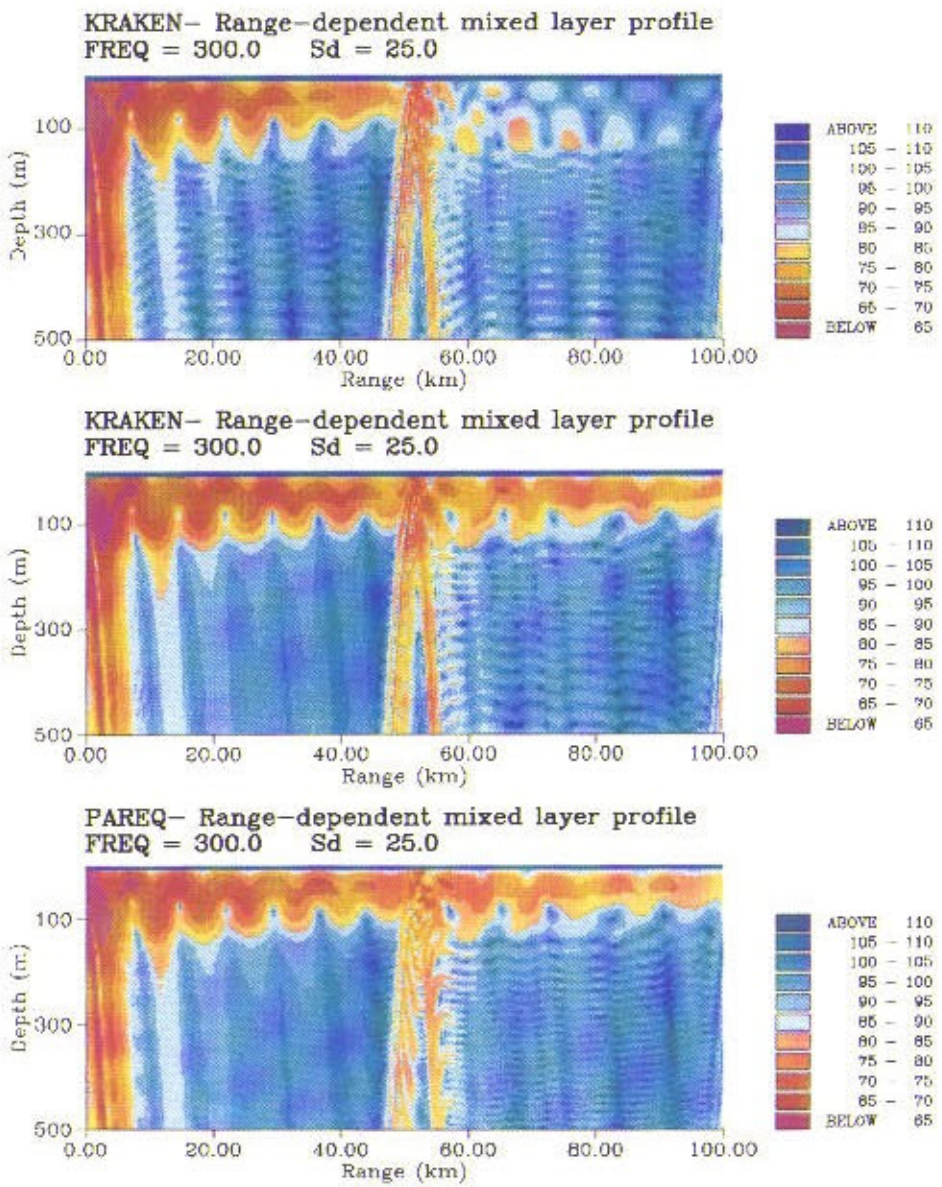

Plate 4. Transmission loss for the range-dependent problem using **(a)** adiabatic mode theory, **(b)** coupled mode theory and **(c)** PE. *(Black and white version of figure available on p. 63.)*

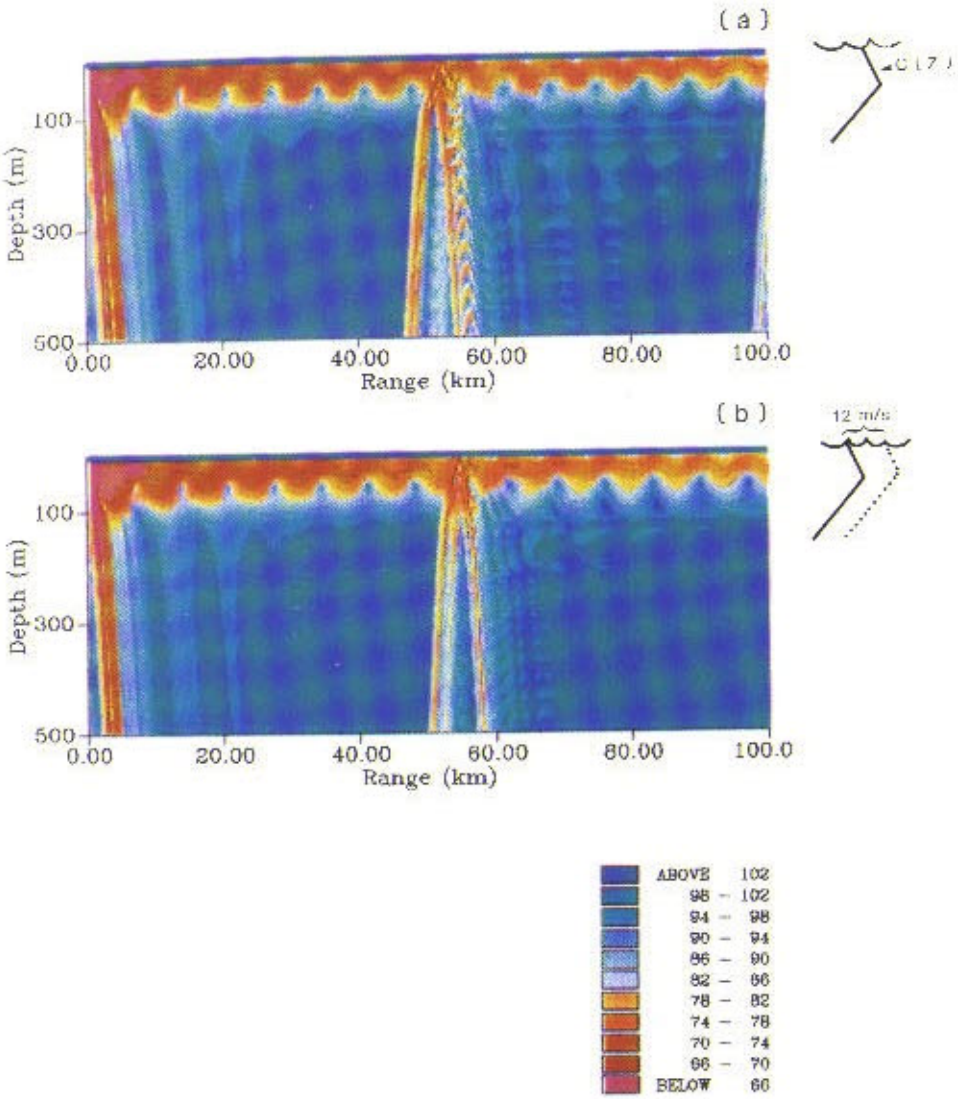

Plate 5. Transmission loss calculations for (**a**) reference profile and (**b**) profile with mixed-layer offset by 12 m/s. (The inset indicates schematically the difference between the perturbed profile (dotted) and reference profile (solid).) (*Black and white version of figure available on p. 65.*)

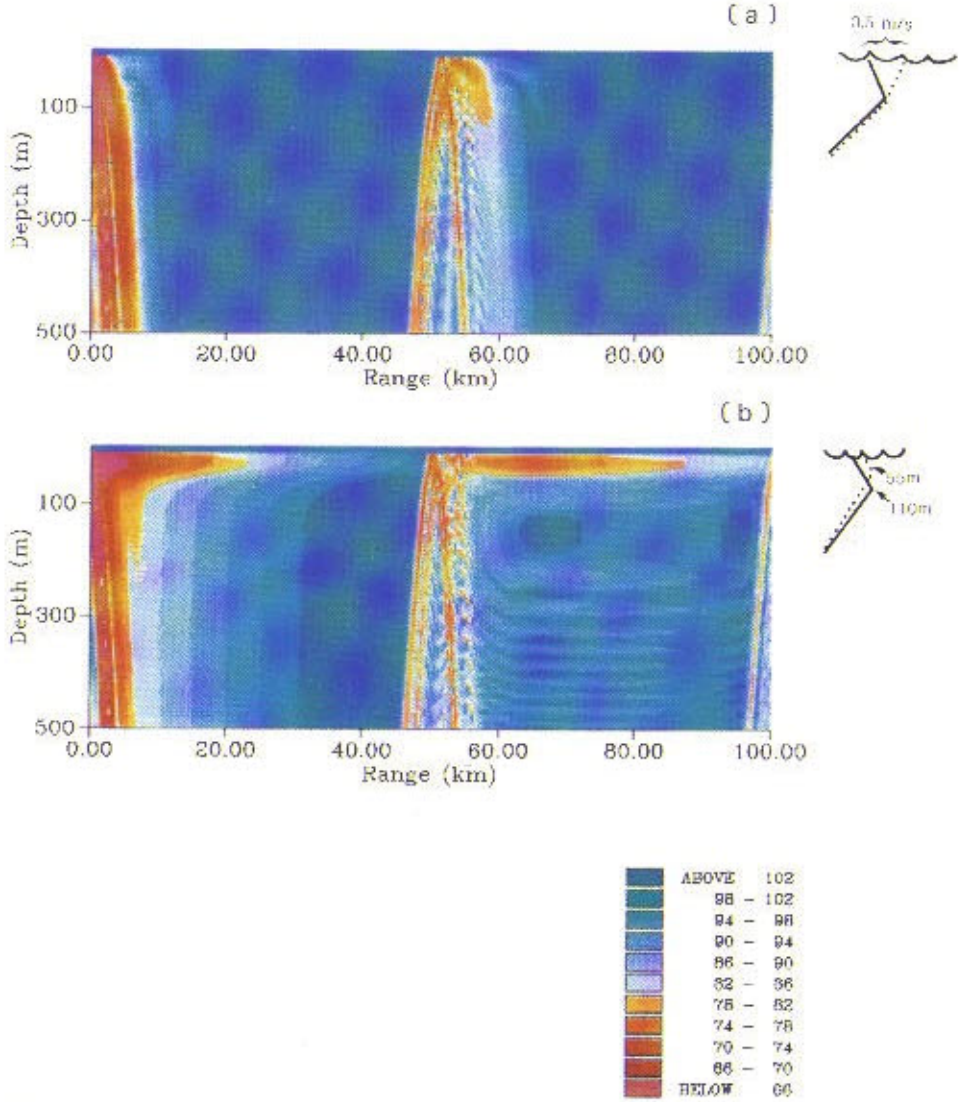

Plate 6. Transmission loss for (**a**) profile with mixed-layer gradient changed to -.016/s and (**b**) to 55 m. (The inset indicates schematically the difference between the perturbed profile (dotted) and reference profile (solid).) (*Black and white version of figure available on p. 66.*)

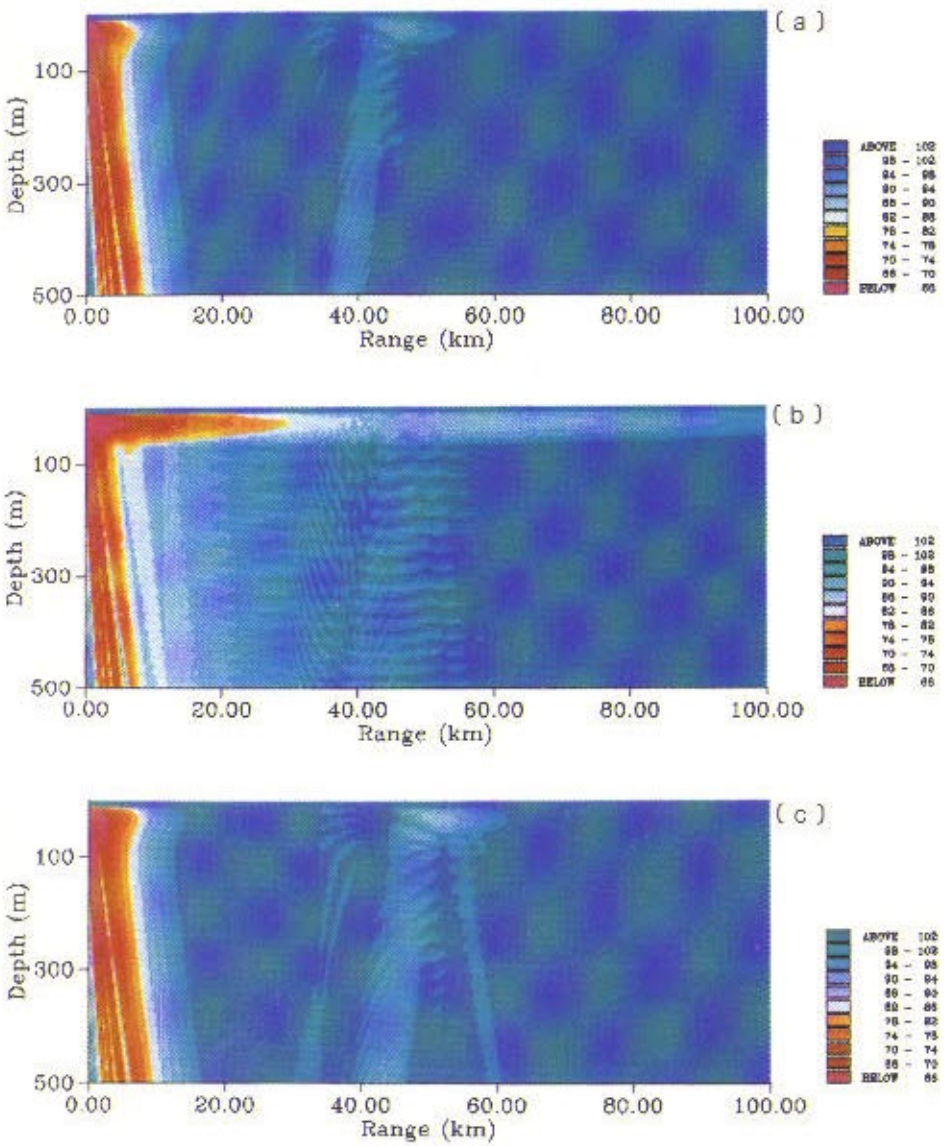

Plate 7. Transmission loss on September 8 using (**a**) experimental measurements, (**b**) ML model and (**c**) climatology for sound speed profile. (*Black and white version of figure available on p. 69.*)

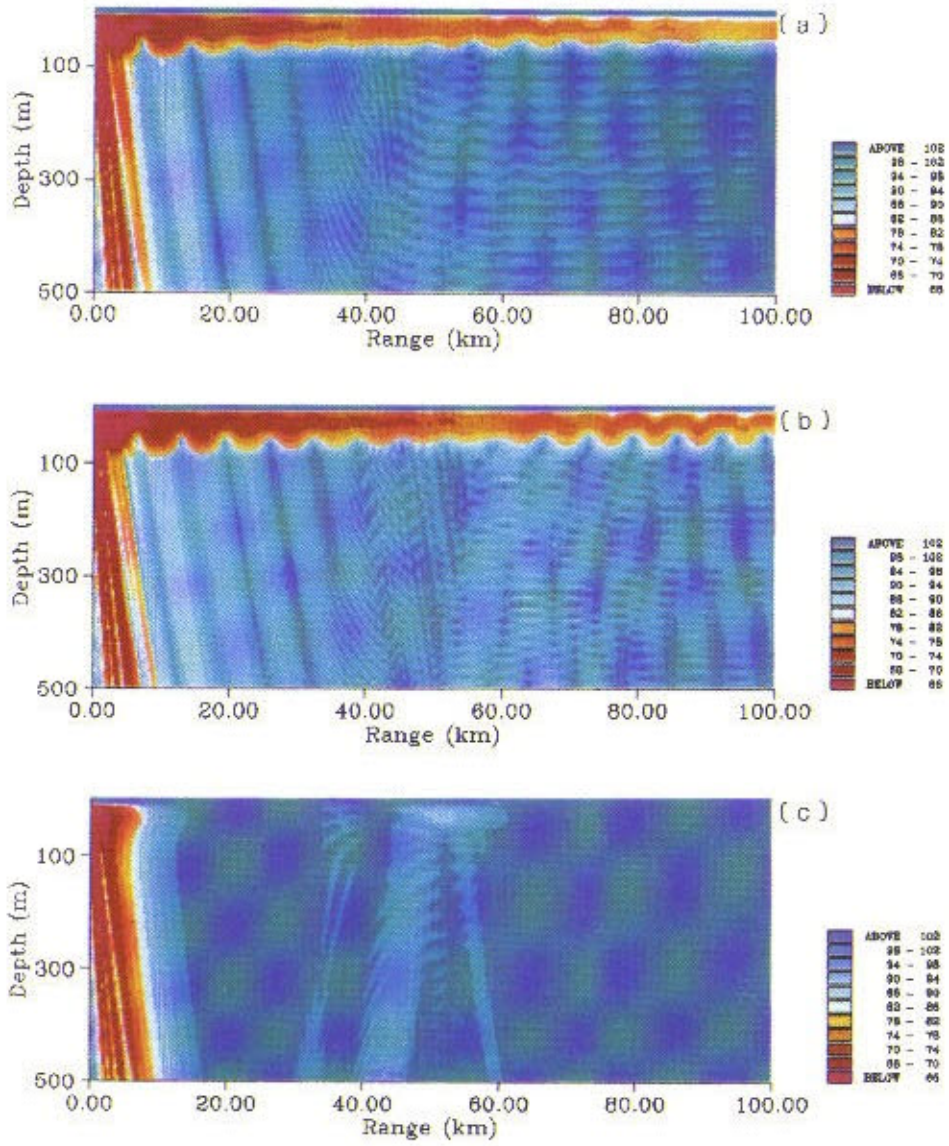

Plate 8. Transmission loss on September 20 using (**a**) experimental measurements, (**b**) ML model and (**c**) climatology for sound speed profile. (*Black and white version of figure available on p. 70.*)

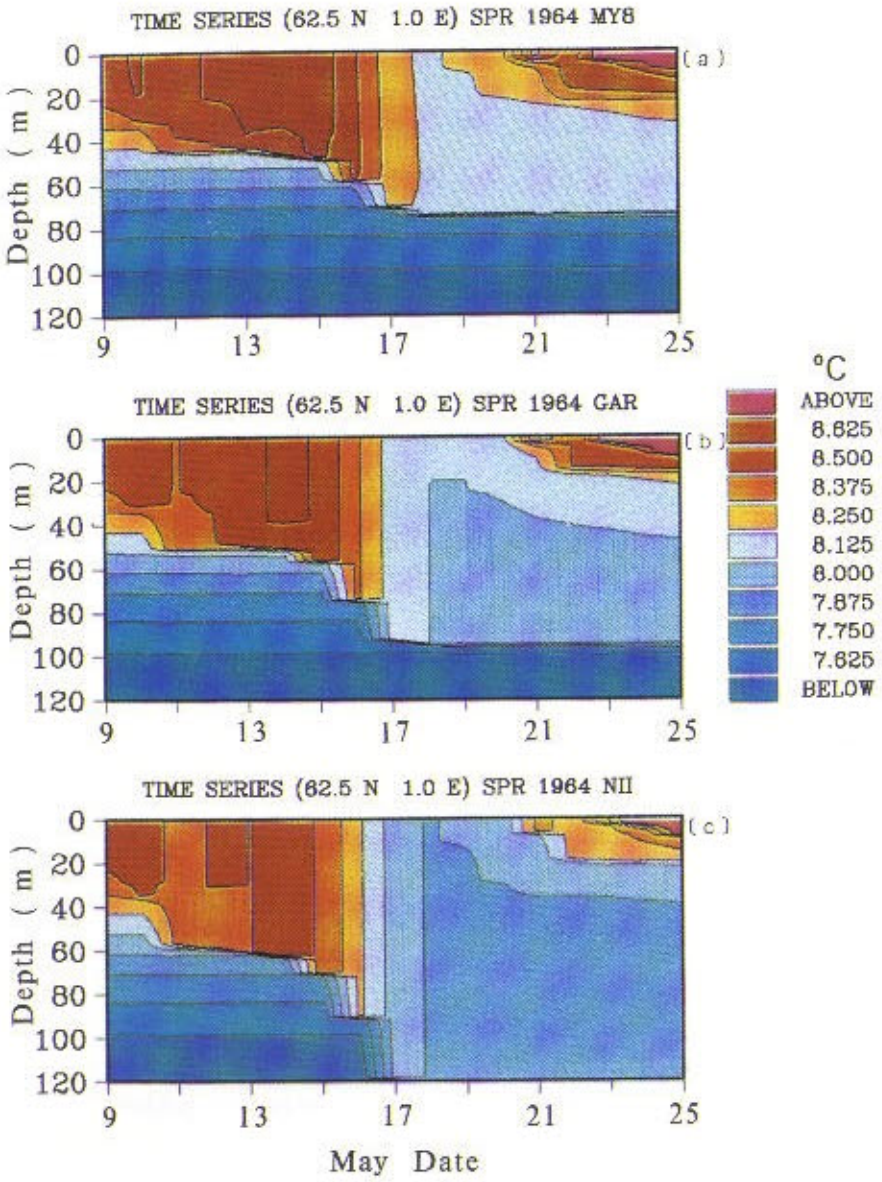

Plate 9. Evolution of the mixed-layer temperature calculated using (**a**) Mellor-Yamada Level 2.5, (**b**) Garwood and (**c**) Niiler models. (*Black and white version of figure available on p. 72.*)

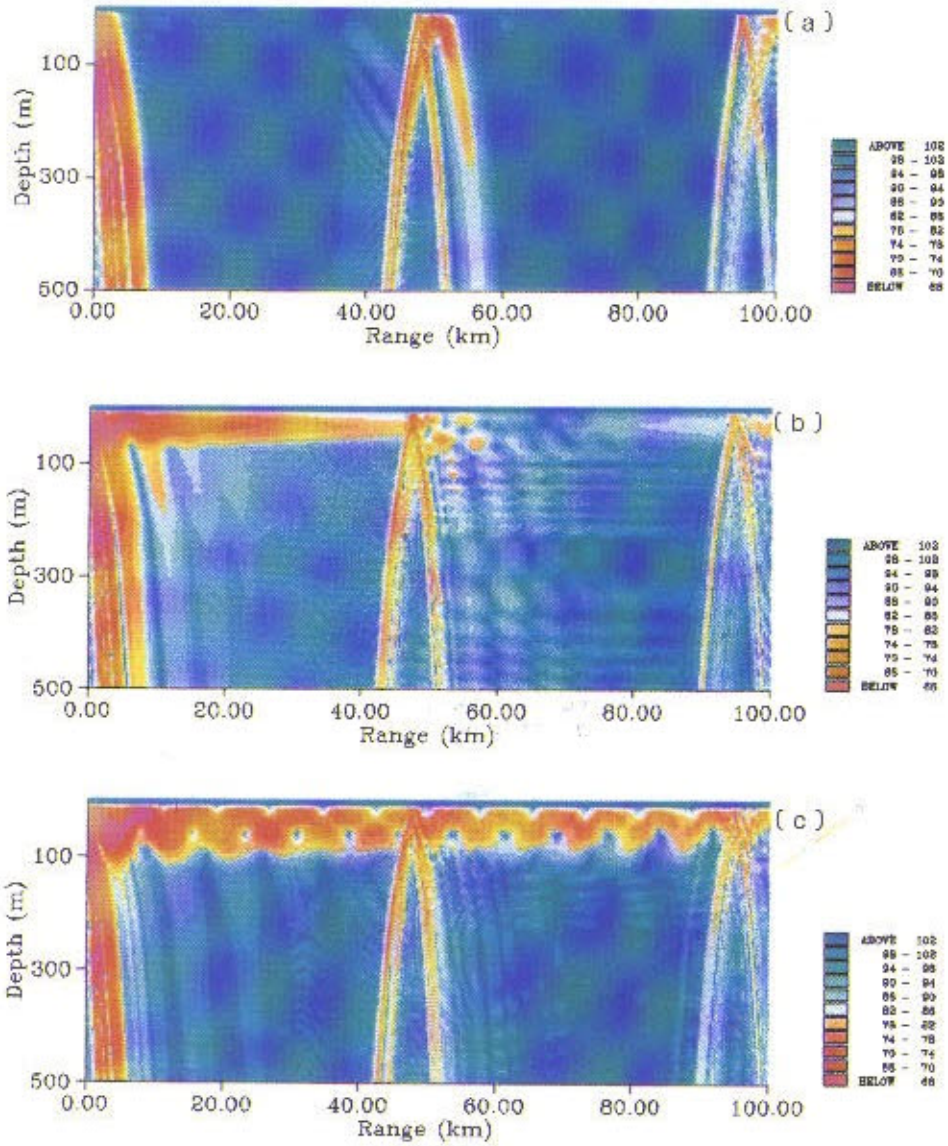

Plate 10. Transmission loss on May 19 (day 8) using (**a**) the climatology initial condition, (**b**) Mellor-Yamada Level 2.5 MLM and (**c**) Niiler MLM for the mixed-layer profile. (*Black and white version of figure available on p. 74.*)

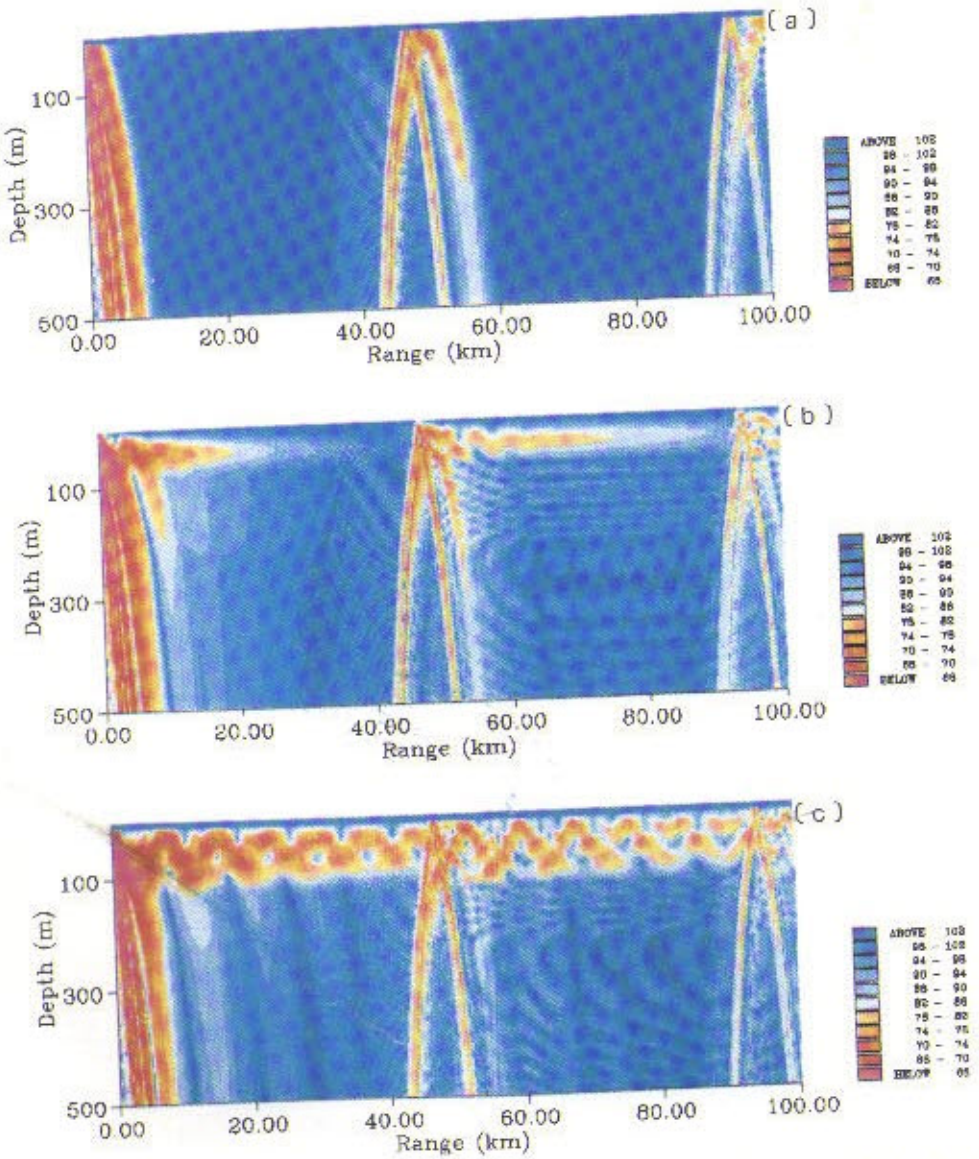

Plate 11. Transmission loss on May 23 (day 12) using **(a)** the climatology initial condition, **(b)** Mellor-Yamada Level 2.5 MLM and **(c)** Niiler MLM for the mixed-layer profile. (*Black and white version of figure available on p. 75.*)

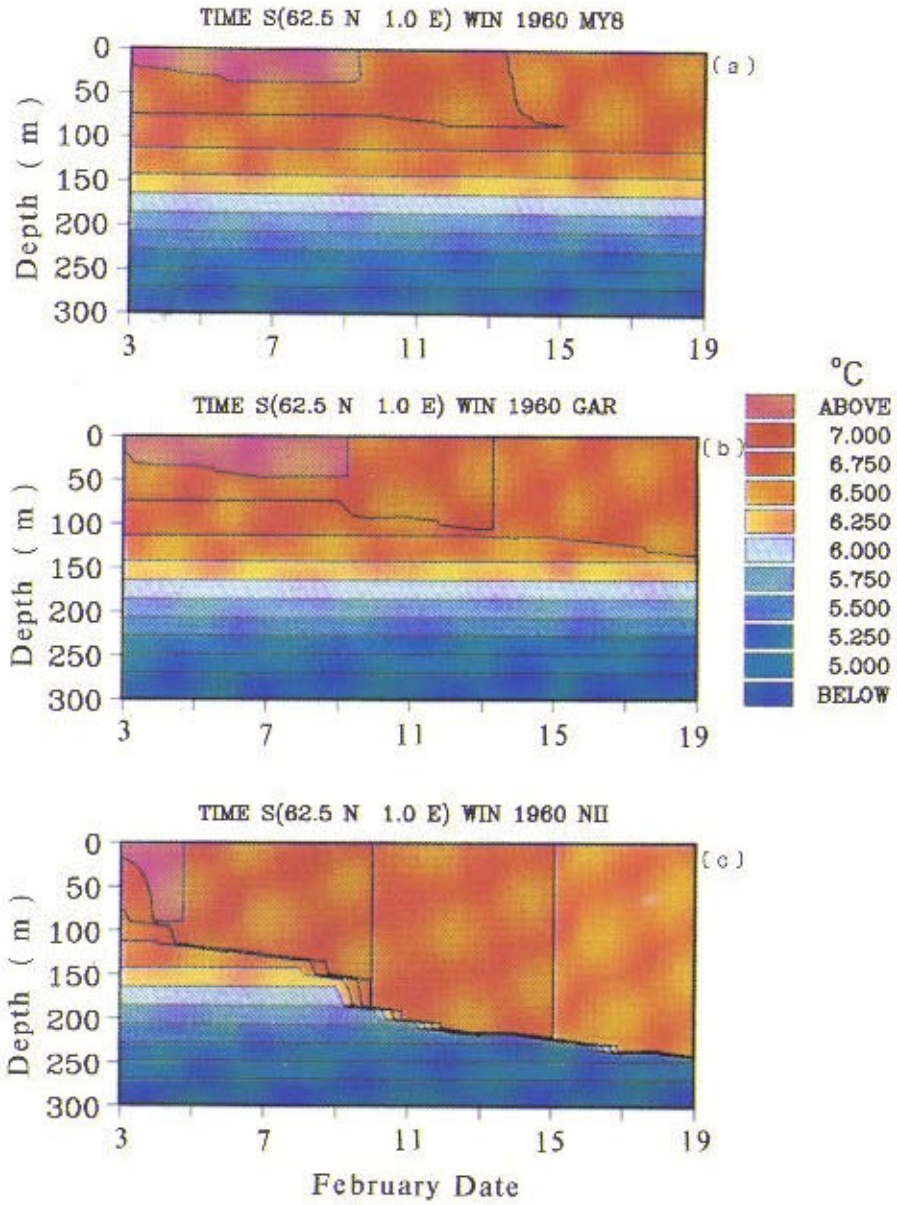

Plate 12. Evolution of the mixed-layer temperature calculated using **(a)** Mellor-Yamada Level 2.5, **(b)** Garwood and **(c)** Niiler models. (*Black and white version of figure available on p. 77.*)

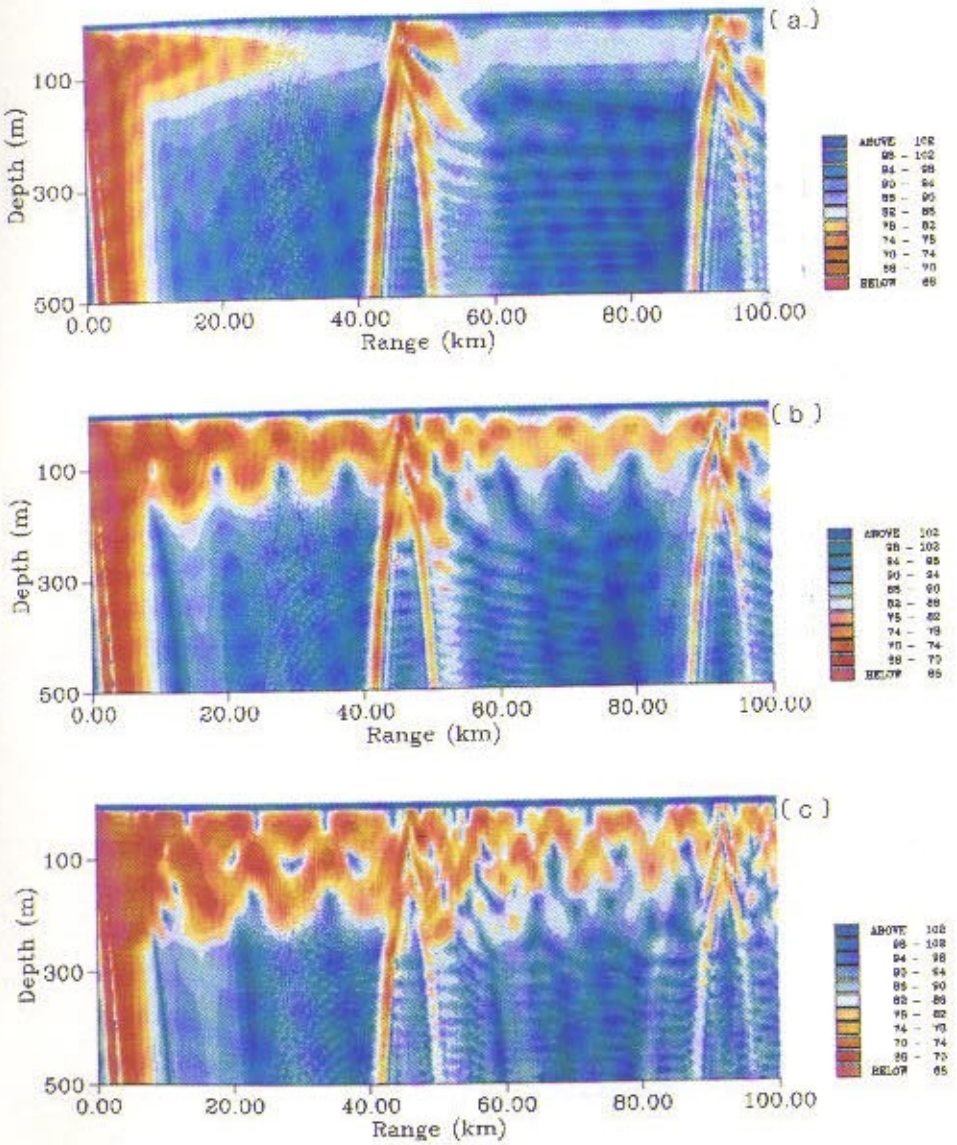

Plate 13. Transmission loss on February 18 using **(a)** the climatology initial condition, **(b)** Mellor-Yamada Level 2.5 MLM and **(c)** Niiler MLM for the mixed-layer profile. *(Black and white version of figure available on p. 78.)*

is found to have a profound influence on the predicted acoustic propagation for certain frequency and source/receiver depths. In general, the MY2.5 model creates the shallowest mixed layers, and the Niiler model the deepest ones, with the Garwood model yielding intermediate values.

Finally, we have shown that in the winter significant ducting occurs for frequencies as low as 200 Hz, and in the spring as low as 600 Hz.